The Development of a DC Micro-grid model with Maximum Power Point Tracking for Waste Heat Recovery Systems

BY

AHMED ABDELAZIZ ELRAKAYBI, B.Sc.

A thesis

Submitted to the department of Mechanical Engineering and the School of Graduate Studies of McMaster University in partial fulfilment of the requirements for the degree of

Master of Applied Science

Master of Applied Science (2018) McMaster University

(Mechanical Engineering) Hamilton, Ontario, Canada

TITLE: The Development of a DC Micro-grid with Maximum Power Point Tracking for Waste Heat Recovery Systems

AUTHOR: Ahmed Abdelaziz Elrakaybi

B.Sc., (Mechanical Engineering)

Ain Shams University, Cairo, Egypt

SUPERVISOR: Dr. James Cotton

NUMBER OF PAGES: XI, 82

Abstract

Research in sustainable energy sources has become the interest of many studies due to the increasing energy demand and the amount of wasted energy released from existing methods, along with their effect on climate change and environment sustainability. Thermo-Electric Generators (TEGs) are a potential solution that is being studied and implemented as they can convert low grade thermal energy to useful electrical energy at various operating conditions.

The integration of a TEG within a heat exchanger (TEG/HX) system connected to an electrical DC micro-grid, using a Maximum Power Point Tracking (MPPT) system is the focus of this study. Using a numerical TEG/HX model from a previous study and a developed DC micro-grid model the interaction between the thermal and electrical aspects were investigated with the focus on the electrical performance of the system.

The main concern of this study is to investigate the effect of the sub components of the DC micro-grid on the overall available energy. An analytic model was developed to estimate the power loss in the electrical circuit of the micro-grid, the model utilizes the equations for switching and conduction losses which have been used by several studies. Other variables such as the battery characteristics and electrical load profiles were also investigated by simulating several case studies including changing operating conditions.

This study shows the effect of a TEG configuration on the power loss in an electrical system using power loss curves in comparison with the Open Circuit Voltage (OCV) of such configuration. It also covers important modes of operation for the battery, loads and MPPT for a stable and reliable operation of an isolated DC micro-grid system were TEGs are the only source of power.

The result of the study presented is a system design that is able to maximize the electrical energy harvested from the TEGs to extend the operation of the dc-micro-grid first by applying a suitable TEG configuration and consequently a suitable electrical circuit. Secondly, by adapting to the changing operating conditions of the TEGs and the loads; and compensating for these changes using the battery storage system.

Nomenclature

Variables

α	*Seebeck Coefficient*	$[V/°K]$
Δ	*Change/ Difference*	
c	*charge rate for batteries*	*[A.h.]*
STATE OF CHARGE LIMIT%	*Depth of Discharge percentage*	
D	*Duty Cycle*	
E	*Energy*	*[Joules or W.h.]*
f_s	*Switching frequency*	*[Hz]*
I	*Current*	
P	*Power*	*[W]*
pc	*Peukert Coefficient*	
Q	*Charge*	*[Columbs C]*
R	*Resistance*	$[Ohms\ \Omega]$
t	*Time or period*	*[sec.]*
τ_s	*Sampling time*	*[sec.]*
T	*Temperature*	$[°C\ or\ °K\ ]$
V	*Voltage*	*[V]*

Subscript

a	*Actual value*
B, Bat	*Battery*
Cond., C	*Conduction or conduction losses*
D, d	*Diode*
DS	*Drain-Source*
Emf	*Electromotive force*
f	*Diode forward or on state*
fv	*voltage fall time*
In	*input value*
Initial	*initial value set by the controller or MPPT*
Int	*Internal*
L	*inductor*
Load	*At the load side*
Losses	*Total Losses*
M, m	*MOSFET*
Max	*Maximum value or output reached by the MPPT*
n	*Nominal value*
OC	*Open Circuit*
Off	*The semiconductor device is in off state*
On	*The semiconductor device is in on state*
Out, o	*output value*
P	*Period*

percent	*Current or Voltage ripple percentage*
P-N	*P-type N-type couple*
Ref	*Reference for controller or Maximum Power Point Tracker (MPPT)*
ri	*current rise time*
rms	*Root mean square value*
rr	*Reverse recovery*
Sw	*Switch*
TEG	*Thermoelectric Generator*
th	*Threshold value*
utilized	*Energy utilized by the loads*

Contents

List of Figures

List of Tables

Chapter 1

Introduction

A wide range of industrial and commercial applications use heat from resources such as fossil fuel combustion for their main processes. This is not only a source of emissions that contributes in global warming, but it is also not efficient because of several reasons such as: the mechanical and thermal limitations of the applications; and the energy losses during transmission, conversion or storage [1] [2].

The world has started to realize that they need to be conscious about energy usage. This has led research into two directions. The first is to shift the reliance from fossil fuel-based energy resources to more sustainable options like renewable sources. And the second is to reduce the energy waste from current heat sources in applications by using Waste Heat Recovery (WHR) systems.

Waste Heat Recovery projects however are not as developed compared to renewable energy projects. This is because the lower return on investment due to the variability in the processes and the operating conditions; and the increased complexity in implementing such projects [3].

Thermoelectric Generators (TEGs) are a potential solution that have been researched significantly due to their ability to operate under a wide range of temperatures and their ability to be integrated or retrofitted into existing systems. TEGs are solid state devices which require low to no maintenance and are manufactured as modules with different sizes, making them able to be adapted into many systems and designs [4].

One of the applications where TEGs can perform well in a Waste Heat recovery system is gas fired appliances in restaurants such as ovens. Cooking ovens can generate a considerable amount of waste heat during its operation to maintain the required cooking temperature and heat transfer conditions. For a conventional oven about 10% of the heat is used in cooking while the rest is exhausted to the atmosphere [5].

This work is a part of a large Waste Heat Recovery (WHR) project referred to as Thermal-Electric Generator Pizza Oven Waste Energy Recovery (TEG POWER) [5] where a WHR system was developed to harvest the heat lost from conventional cooking ovens. The energy is utilized to provide the thermal energy for space heating using hot water and provides an additional benefit of resiliency to the restaurant by generating electricity to an isolated DC micro-grid system of electrical loads using TEGs as the source of electricity.

For the project, commercial flat TEG modules where implemented in a heat exchanger. The flat TEGs generate electricity while the heat exchanger provides thermal energy to a cooling loop connected to a hot water storage. The TEG system was able to operate at an efficiency of 2% from the waste heat generated generating a power of 79W. The TEG system consisted of 24 modules each having 126 couples connected electrically in series. The TEGs were originally connected to a commercial Maximum Power Point Tracker (MPPT) developed for Photovoltaic (PV) systems to maximize the power being generated given the electrical characteristics of the TEGs “load matching” between the TEG system and the electrical loads under different operating conditions. The loads on the DC micro-grid includes a battery storage connected in parallel to a fan and two alternating pumps which were used to run the cooling system along with other restaurant loads such as LED lighting, the WI-FI and point-of-sale system.

Further next generation TEG POWER system is being studied [6], a new heat exchanger design has been developed where it is intended to use annular TEG couples instead of the commercial flat TEGs to generate power. The new TEG design has different Voltage Current (V-I) characteristics and through system integration the performance of the heat exchanger can be

improved. They can be easily implemented in the new heat exchanger and other similar systems due to their annular shape.

One of the goals of the current project is to improve over the current system by maximizing the electrical energy harvested to extend the time the DC-micro-grid system can operate. Accordingly, this research will involve the study of key parameters in the systems such as the various ways to electrically connect a TEG array together to achieve a certain power level, the impact of each array configuration on the DC micro-grid and the different MPPT circuit configurations. In addition, for reliability and stability purposes in the DC micro-grid, an energy storage and management system are developed where the system becomes fully automated and able to react to different scenarios which will ensure the restaurant resiliency.

1.1 Objectives

The objective of this work is to study the effect of the TEG system V-I characteristics on the electrical system consisting of the MPPT, electrical loads and battery storage using a power loss model to estimate the switching and conduction power losses for the electrical system. The model connects to the TEG heat exchanger thermal performance model developed [6] for the next generation TEG modules using MatLab. Different operating conditions are being tested based on planned restaurant operation modes to predict the overall system performance and efficiency including the MPPT, energy storage system and the micro-grid.

An electrical DC micro-grid is designed to harvest as much electrical energy possible by developing an energy management system that balances the micro-grid energy demand and storage to compensate for the energy excess and needs during different operation modes. The components of the micro-grid include the MPPT, the energy storage; and the loads given by a demand profile representing common consumption patterns in restaurants.

1.2 Scope of Work

The scope of this work is to perform a case study to investigate the ability of the model to control the performance of the dc-micro-grid and protect the battery system while efficiently utilizing the energy generated from the TEG system. Daily performance of a DC-micro-grid system under different modes of operation is predicted to study the effect of the different V-I characteristics of the thermoelectric generators on the MPPT system performance by modeling the electrical losses of different MPPT and TEG configurations. The TEG operation along with the MPPT circuit design and algorithm that effect the performance of the electrical losses and efficiency are studied.

1.3 Thesis Outline

The thesis is divided into five chapters including this one which is the introductory chapter. The second chapter gives a general overview for thermoelectric generators, the operation of dc-microgrids, maximum power point trackers, DC converters and energy storage systems such as batteries.

Chapter three discusses in detail the modeling of the DC- microgrid components such as thermoelectric generator/ heat exchanger system, the maximum power point tracker, the DC-converter and the associated power losses; and the algorithms used to operate the system battery system, load shedding and energy management.

Chapter four shows the results of the developed model as well as two case studies and discusses the results such as the effect of choosing a thermoelectric configuration on power losses, the effect of changing the battery capacity on the energy utilized by the DC- microgrid and how the system reacts when conditions such as energy shortage or load shedding are required.

Chapter five is the thesis conclusion and summary, it also discusses some recommended future work based on this thesis.

1.4 Summary of contributions

The model developed in this study can be used in selecting a TEG configuration based on the power loss model for the DC converter. It is also able to take into consideration all the system losses starting from the heat exchanger to the loads and simulate the system losses at each stage. This is beneficial in providing estimates for real systems perfromance in similar applications to determine their feasibility.

Chapter 2

Literature Review of Thermoelectric Generator based DC-microgrids

2.1. Introduction

The TEG POWER system consists of a heat exchanger mounted on the exhaust of an oven, the TEG modules are implemented and clamped inside the heat exchanger. The TEG/Heat exchanger system (POWER system) generates electrical power to a DC micro-grid and provides heat to a separate thermal storage system. This study is concerned with the electrical part of the project.

Figure (1) shows a simple representation of the DC micro-grid. The POWER system is connected to a Maximum Power Point Tracker (MPPT) to operate at maximum power. The MPPT provides the power to the rest of the grid through a 12V DC bus which is connected to the loads and the energy storage system.

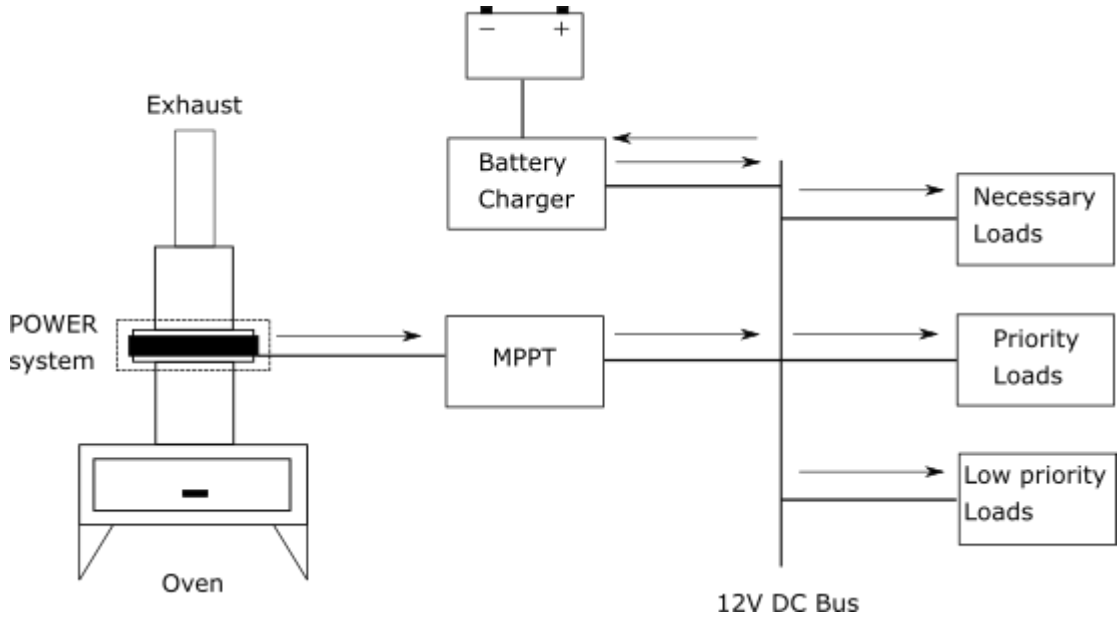

Figure 1: Simple representation of the TEG POWER DC micro-grid.

The literature review chapter is divided according to the components of the DC micro-grid: The TEG system, the MPPT algorithm, the electrical circuitry, the Energy Storage System (ESS) and the Energy Management System (EMS).

2.2. Thermoelectric generators characteristics and operation

2.2.1. Theory of operation

When thermoelectric generators are considered for electric power generation the main thermoelectric effect responsible for the TEGs electrical performance is the Seebeck effect [4]. The Seebeck effect can be described using Figure (2), it represents a circuit formed from two dissimilar metal conductors. The thermoelectric legs or elements (a & b) are connected electrically in series and thermally in parallel to the two junctions (A & B) which are maintained at different temperatures T_A and T_B where for example ($T_A > T_B$). The result is an electromotive force generated between the junctions (C & D). The Seebeck effect can be described using equation 2.2.

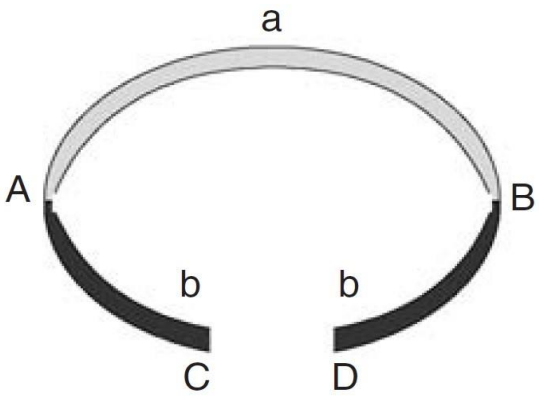

Figure 2: Schematic of a Basic Thermocouple

$$V_{emf} = \alpha\,(T_1 - T_2) \tag{2.1}$$

$$\alpha = \frac{V_{emf}}{\Delta T} \tag{2.2}$$

Where α is the Seebeck coefficient. Equation 2.2 describes the magnitude of the voltage produced by two junctions of two dissimilar materials generate with temperature difference. The Seebeck coefficient is different depending on the materials used where the higher the value the more voltage said material can generate.

It is possible to alter the performance of these materials using dopants. A semiconductor material can be doped to be N-type with a negative Seebeck coefficient forming the first junction, while the second junction can be doped to a P-type with a positive Seebeck coefficient. The Seebeck coefficient for this circuit is then improved, this is how Thermoelectric couples are built. Connecting multiple thermocouples (*N*) electrically in series changes the equation 2.3 to:

$$V_{emf} = N\alpha_{P-N}(T_1 - T_2) \tag{2.3}$$

Figure (3) shows a TEG module consisting of N number of couples operating under a temperature gradient where the temperatures are constant on the hot and cold sides, labeled as T_H & T_C respectively.

2.2.2. V-I and P-V characteristics of Thermoelectric generators

A voltage V_{OC} is generated due to the temperature gradient on a TEG module, when connecting the TEG module to a load resistance R_L, a current I will flow through the circuit, the voltage output at the load side is:

$$V = V_{OC} - IR_{TEG} \tag{2.4}$$

Where R_{TEG} is the electrical resistance of the semiconductor couples. The V-I relation for the TEG is a linear relation as shown in equation 2.4 and the power generated by the TEG module P_{TEG} is as equation 2.5. This is depicted in Figure 3 and 4, where it shows the equivalent electrical representation of a TEG system.

$$P_{TEG} = IV_{OC} - I^2R_{TEG} \tag{2.5}$$

If equations 2.4 and 2.5 are plotted against the current I which ranges from zero to the short circuit current I_{SC}, the Voltage-Current (V-I) and the Power-Current (P-I) characteristic curves for the TEG module are obtained as in Figure (4).

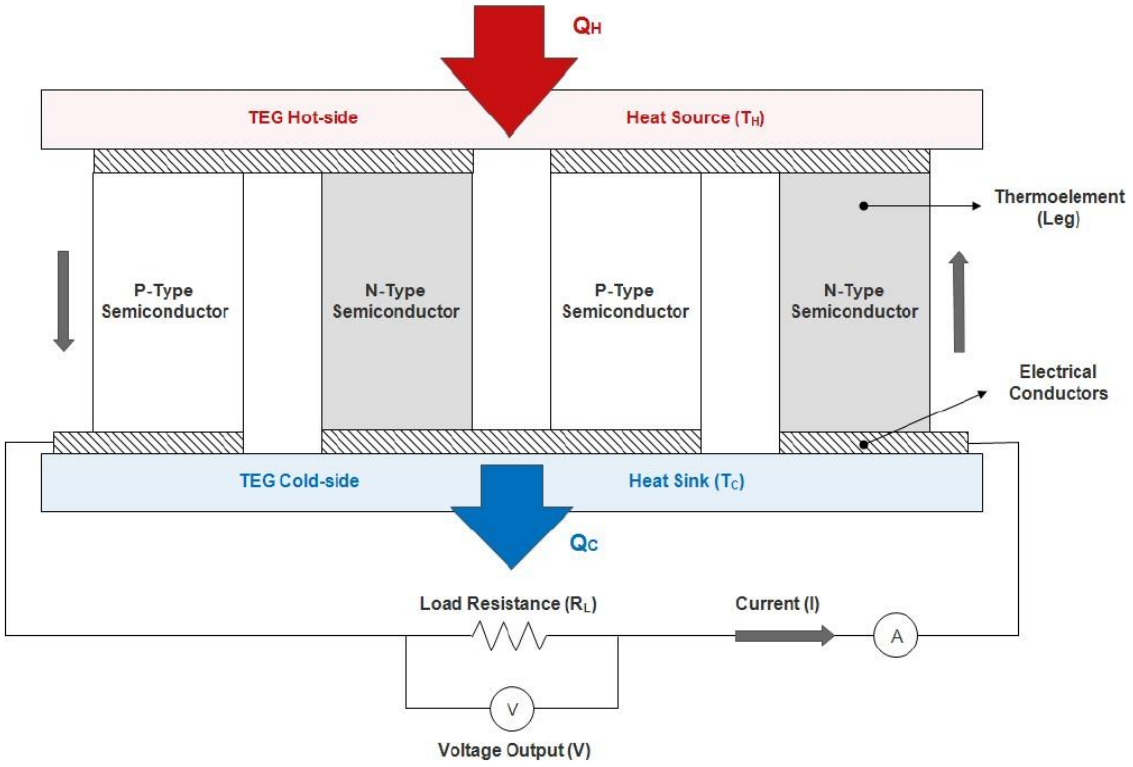

Figure 3: Thermoelectric Module Operating Under a Temperature difference.

To operate the TEG module at maximum power it should operate at a voltage equals to half its open circuit voltage. From substituting with this voltage value for the current and in equation 2.4.

$$I = \frac{V}{R_{Load}} = \frac{\frac{1}{2}V_{OC}}{R_{Load}} \tag{2.6}$$

$$\frac{1}{2}V_{OC} = V_{OC} - IR_{TEG} \tag{2.7}$$

$$R_{TEG} = R_{Load} \tag{2.8}$$

It is evident from the relations discussed that to extract the maximum power available from a TEG module the electrical circuit must be designed to match the resistance of the TEG module or array in case of multiple modules. In a real-life application this is difficult to achieve due to the dynamic conditions that effects a TEG based system operation. Also, a single module does not usually provide enough energy and multiple TEG modules are electrically connected in an array to accumulate energy from each TEG. To extract the maximum energy from such array and to achieve load matching a maximum power point tracker (MPPT) is electrically connected to it.

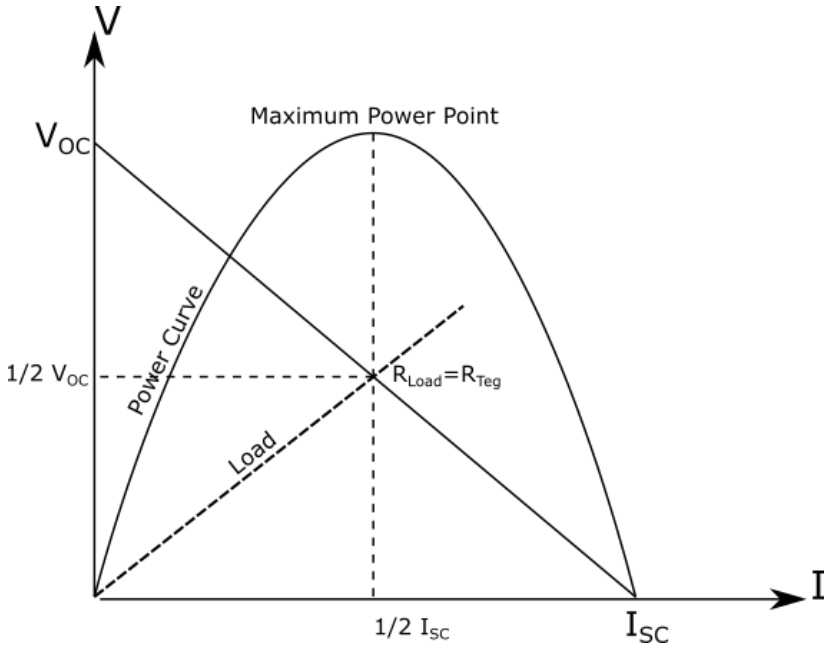

Figure 4: V-I and P-I Trends for a TEG module.

2.2.3. Mismatch and electrical configuration power losses

The MPPT used for such arrays will only give a satisfactory performance provided that each TEG module in the array operates under the same parameters. Such parameters are a function of the intrinsic properties of the TEG module itself, as it is impossible to have identical TEG modules due to manufacturing tolerance and material variability [7]; and the operating conditions for each module in the array, for example due to temperature or flow maldistribution.

Any differences in such parameters will cause a mismatch between the modules in the array which results in different maximum power points. The combined maximum power point of such array will be less than an ideal case where all parameters are the same for each TEG module.

The main reason for the mismatch in case of thermoelectric generators is the temperature gradient applied on an array of TEGs connected electrically together. For example, when the TEG array is implemented inside a heat exchanger or an automotive exhaust system[8]. Each individual TEG module in such case provides a power output different from the rest of the TEG array. And if only one MPPT is connected to the whole array, some of the TEGs will not be operating at their maximum power.

The electric connection between the TEG modules combined with such mismatch also contributes to the overall power losses, this is because the electrical Joule heating losses resulting from the combined TEG modules.

For the first generation TEG POWER [5], [6], commercial flat TEGs were implemented in a heat exchanger setup. The hot side of the TEGs being heated by the oven's exhaust gas while the cold side cooled by propylene glycol/ water mixture. The mismatch effect was not thoroughly investigated as there was only temperature readings at the inlet and outlet of the heat exchanger and the temperature gradient could not be determined.

The second generation TEG POWER annular TEGs setup [6] on the other hand was modeled and validated. Four rows of TEGs connected in series and parallel were tested in this model. Depending on the temperature gradient for the heat exchanger the effect of mismatch has been studied for two electrical connections between the TEG rows, series and parallel

Figure (5) shows the temperatures of the outlet exhaust gas at each TEG row, the water outlet and the hot side and cold side temperature gradients from the annular TEG model [6].

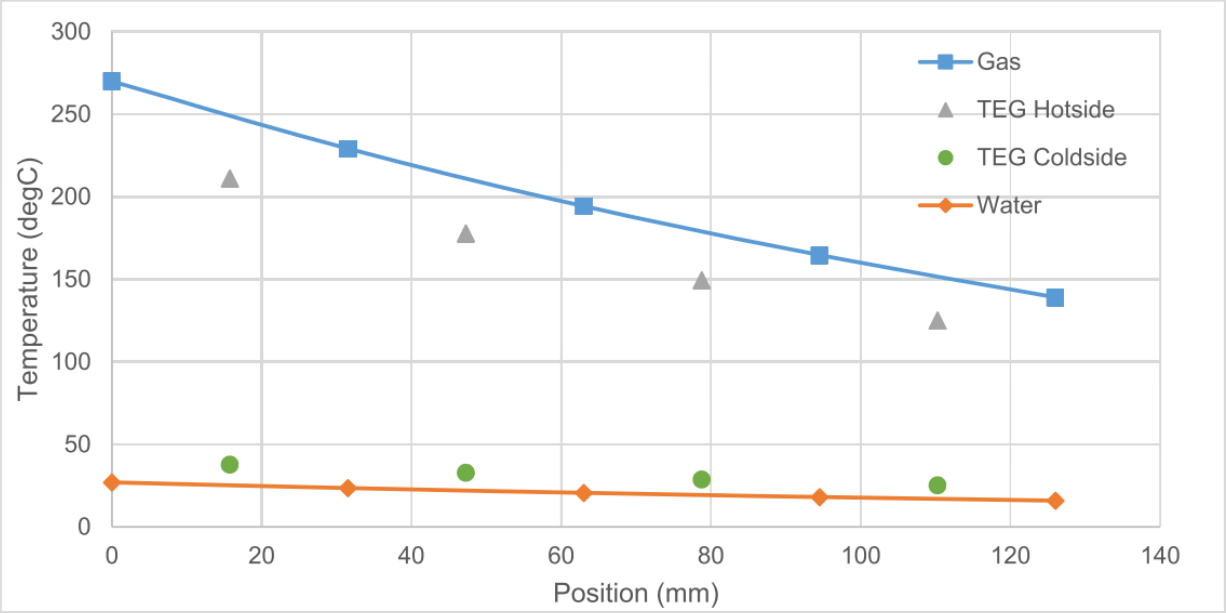

Figure 5: The temperature variation of gas, water, TEG hot-side and cold-side surfaces along the heat exchanger length [6].

The result of this simulation was 1.1% loss of power in the series configuration due to mismatch, for the parallel connection case the losses reached 5%. From this result the series connection seems to have lesser losses due to temperature gradient mismatch. Similar conclusions on mismatch can also be found from literature:

A. Montecucco [9] studied the effect of temperature mismatch for three TEGs. The temperature difference between the hot and cold side for each TEG were 100 °C, 150 °C and 200 °C respectively. They compared the combined power outputs at the maximum power point when the TEGs are connected electrically in series and parallel to their ideal cases. They found out that for the series connection case the power was 9.22% less than the ideal power due to mismatch while for the parallel case the power was 12.9% less. They also showed the possibility of the TEGs to operate with negative current or heat pumping mode for the high mismatch temperature. They concluded that a series connection is generally a better connection to reduce the power losses.

Tang. Z. B. [8] tried to emulate the effect of mismatch in for automotive applications. He implemented a string of six TEGs in a series connection over an exhaust pipe of a two-liter engine. While the cold side was kept at a constant 90 °C, the hot side of the TEG string experienced a temperature gradient as the temperature decreased from the inlet of the exhaust to the outlet. The starting inlet and outlet temperature and the temperature gradient were also a function of the engine speed (i.e. gas mass flow rate), at 3400 RPM the power loss due to the mismatch between the TEG string was found to be around 11%. He also tested the effect of clamping pressure mismatch on individual TEGs. By applying three different masses of 60, 120 and 180 kg on a 50*50 mm TEG surface, the output power at 60kg of the TEG was 8.1% less than the 180 kg case. While it was 2.6% less for the 120 kg.

Other studies investigated variations of TEG configurations on power losses. Negash, A. A. [10] tested ten TEGs in eight different configurations experimentally. By taking the sum of each individual TEG power output as a reference and comparing it with the output of each configuration to conclude which variation minimizes the effect of mismatch. The main parameters for his study was the number of parallel junctions in the configuration and the number of unbalanced strings where some strings are made up of different number of TEG modules. The results showed that balanced configurations with the equal modules in series and parallel; and having the least number of junctions were the most efficient in minimizing the mismatch losses.

Thankakan, R. [11] derived an analytical model for TEG modules connected in different configurations under homogenous and heterogenous temperature gradients. Like other studies, the reference power was determined by combining all the individual TEG power outputs and was compared to the power output of various configurations. The first test was comparing five different TEG configurations made up of sixteen TEG modules under a homogenous temperature gradient. He found similar results for the (2x8) (4x4) and (8x2) series-parallel configurations all having an approximate 4.5% loss. However, for large scale systems he stated that a square configuration where parallel and series connections are equal is more suitable as it provides reasonable voltage and current outputs for the MPPT and the DC-micro-grid.

The second test was comparing 3 strings (3 series, 3 parallel or 3 square) made up of 9 TEGs each, then connected in a star configuration, shown in Figure [6]. The star connection was used as a way to provide three different DC outputs to the loads with fewer wires and complexity. The test was divided into two parts the first was applying a homogenous temperature gradient and the second was by applying a heterogenous gradient. The series connected strings performed better than the other configurations for the two tests.

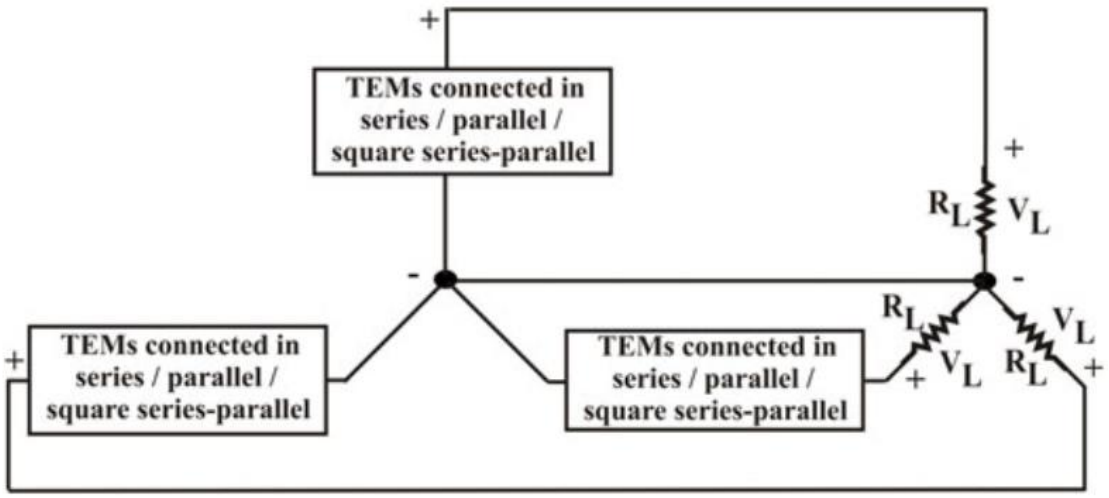

Figure 6: Schematic diagram of various configurations of TEGs in star connection [11].

Photovoltaic (PV) systems deal with similar design problems as the TEG systems. As they are susceptible to a shadowing effect due to the surrounding environment blocking the sun light on parts of the PV panels, this maybe the because of clouds, trees, dust or simply the time of the day. All of these factors decrease the power produced from these panels compared to the rest of the system.

Shadowing in PV systems is widely researched as it is a very common problem. these studies are discussed in a review paper by Bastidas-Rodriguez and E. Franco [12]. The techniques presented were mainly divided into three types: the first is modifying the MPPT algorithm, the second is modifying the converters type or number and how they are connected to the PV system; and

the third is changing the electrical connections between the panels of an array or between different ones. Most of the solutions studied for PV systems are also viable for TEG systems as both systems are implemented in similar fashion electrically, for example Zhang [13] used a hybrid TEG and PV WHR system for a vehicle, he used the same power converter for both systems. There was a power difference however, so he treated them as two mismatched modules. He also used the same MPPT to track either the TEG and the PV systems.

However, as stated earlier the mismatch losses for the TEG POWER second generation model is around 1% or 5% for the two studied cases in TEG POWER. Before designing a solution for the mismatch, determining which TEG configuration to implement is required. This is because some TEG configurations minimizes this effect as shown in literature. However, there are no studies that investigate effect of mismatch on a whole system level where the TEG system is connected to the MPPT and the DC micro-grid. Deciding which TEG configuration to use has more consequences on the overall system performance not just the mismatch losses, as it also contributes in the efficiency of the DC converter inside the MPPT and impacts the choice of converter that should be used to handle the voltage and current output of the TEG system.

For this reason, this study will investigate the relation between the TEG array output power, voltage and current on the electrical power losses of the MPPT and the overall micro-grid system.

Table (1) summarizes some of the literature studies on the TEG array performance when experiencing a temperature gradient and/ or different electrical array configurations.

Table 1: Summary on some studies discussing the effect of temperature mismatch and electric configurations on TEGs.

Author	**TEG array configuration**	**Experimental setup**	**Mismatch temperatures**		**Ideal maximum power**	**Array maximum power**	**Remarks**
			Hot Side	**Cold Side**			
Montecucco, et al. 2014 [9]	3 TEGs in series and parallel.	Test setup to characterize individual TEGs.	ΔT= 100℃, 150℃, 300℃ respectively for TEG# 1 ,2 and 3.		20.07 W	18.22 W for series. 17.48 W for parallel.	Joule heating losses were not quantified.
Tang, et al. 2015 [8]	6 TEGs connected in series.	Test setup to characterize TEGs. Test bench to emulate exhaust system.	Hot side starts highest at exhaust inlet and falls until exhaust outlet on the last TEG. (350℃, -200℃,) at 3200 rpm.	90 ℃.	15.86 W	14.12 W for series	Did not test parallel configurations. Mismatch can be from unequal clamping pressure.
Negash, et al. 2017 [10]	10 TEGs in 8 different config. Combinations of series and parallel.	TEGs attached to exhaust gas channel of a diesel engine. And a chiller for cooling.	327℃ at Steady state. Varying slightly along the TEGs.	10 ℃	34.2 W	32.2W for all series. 30.3 W for all parallel. 32.6W for 2 parallel junctions with 5 TEGs in series.	Losses in configuration with unbalanced junctions. Suggests minimizing the parallel connections.
Thankakan, Nadar. 2018 [11]	16 TEGs in in 5 different config. without a temperature gradient. 3 strings (3 series, 3 parallel or 3 square) made up of 9 TEGs. Connected in a star config.	Test setup to characterize individual TEGs.	ΔT=443 $°K$ ΔT=443 $°K$ homogenous temperature gradient. 50% at ΔT=369$°K$, 25% at ΔT=349$°K$, 25% at ΔT=329$°K$		18.2 W 10.2W 9.2W	17.39 W for (2x8) (8x2) (4x4) series- parallel config., unbalanced config. 9.9W series, 9.7W parallel, 9.8W square. 6.5W series, 6.29W parallel, 6.4W square.	Star connection is viable for large scale TEG arrays with different DC outputs as it decreases the wiring and complexity.

2.3. Maximum Power Point Tracking

The Maximum Power Point Tracker (MPPT) is a device used commonly in application with power sources that have a variable P-V and V-I characteristics. Its purpose is to adjust the operating point of such power sources to always operate at maximum power by changing the load connected to them in a process called load matching or impedance matching. MPPTs can be found in applications where Photovoltaic, Thermoelectric generators or Turbines are used. Although there have been studies about the MPPT since the 80s [14], they didn't represent a feasible solution until recently as the cost electronics and microprocessor chips have decreased.

A MPPT consists of two main parts: the MPPT algorithm and the electrical circuit. The most common MPPT algorithms used are the hill climbing algorithms specifically the Perturb and Observe (P&O) and the Incremental Conductance (Inc.) for their simplicity and efficiency. The algorithm used determines the operation of the electrical circuit which is usually a DC converter or an inverter.

In literature both the algorithms and the electrical circuits for the MPPTs have been extensively studied for different applications and purposes. A comparison of different MPPT algorithms by Esram and Chapman [15] categorizes the algorithms by their major characteristics and a suitable MPPT can be chosen depending on the application. For TEG POWER the required characteristics are as follows:

Array Dependency: This means that if the MPPT will correct itself if the electrical output of the TEG system changes with the changing operating conditions or was the MPPT predesigned to operate in a certain way. An example of Array dependent algorithms is the Fractional V_{OC} [16], Fuzzy Logic control [17] and Neural Networks [18].

Convergence Speed: It is how fast a MPPT will reach the maximum power point. This characteristic is very important in dynamic applications such as automotive WHR. Fortunately, For the application in TEG POWER the system dynamics are very slow which allows the usage of relatively slower algorithms.

Steady State Response [19]**:** It is how accurate the MPPT response compared to the referenced signal when it reaches a steady state. This characteristic is very difficult to characterize as it is dependent on many factors. For hill climbing algorithms for instance, it depends on the size of perturbation and the frequency of the MPPT. The smaller the perturbation, the more accurate the steady state response becomes. On the other hand, the algorithm convergence speed decreases. To overcome this problem, algorithms such as variable step P&O are developed [20].

From literature hill climbing algorithms such as P&O and Inc. seems to perform efficiently specially for applications that do not require high dynamic speed or transients. The application of these simple algorithms is viable given they are properly designed. For this study the P&O algorithm is used.

The operating idea of P&O is simple, it measures the value of the TEG system voltage and current then decides to change the control of the electrical circuit by changing the reference voltage V_{ref} or the duty ratio D. The algorithm changes these values with a fixed step size iteratively where it goes up the power curve as shown in Figure (7). The algorithm however will not reach a fixed maximum power point as it will oscillate around it. To ensure that the algorithm is accurate at steady state, the design method in [21] was followed to properly configure the algorithm to the system.

The next section will discuss the electrical circuits used for the MPPT.

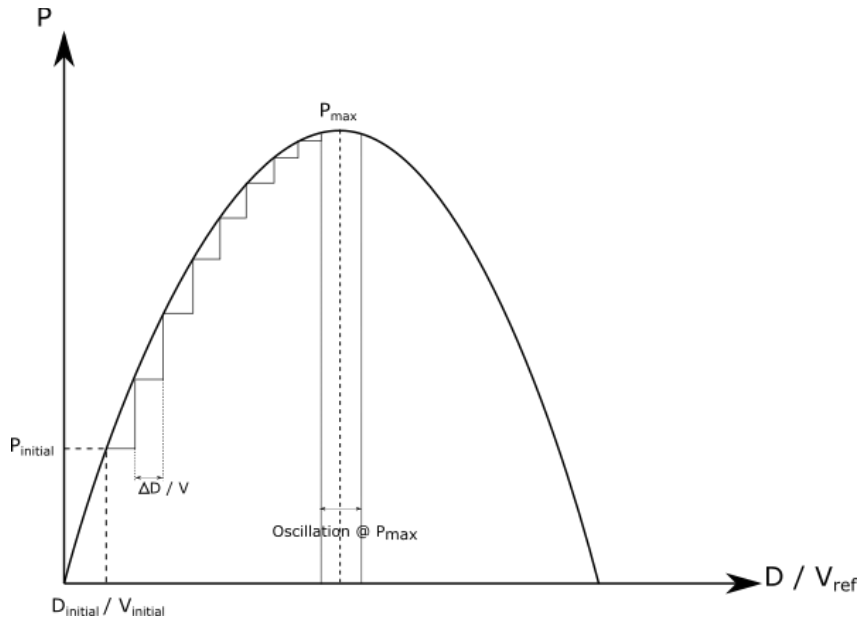

Figure 7: P & O Hill Climbing Principle

2.4. DC Micro-grid Electrical Circuit configuration and Losses

This section discusses the electrical circuits used in the DC- micro-grid, for the islanded grid setup two DC- converters are needed. The first is for the MPPT and the second is for managing the battery. As discussed in the mismatch section, this study will investigate the relation between the TEG array output power, voltage and current on the electrical power losses of the MPPT and the overall micro-grid system. Thus, different types of DC- converters are investigated. For the MPPT three common types of converters are modeled: a buck converter, a boost converter and a SEPIC buck- boost converter, shown in Figure (8) (a) and (b) respectively. The theory of operation for these DC converters can be found in [22].

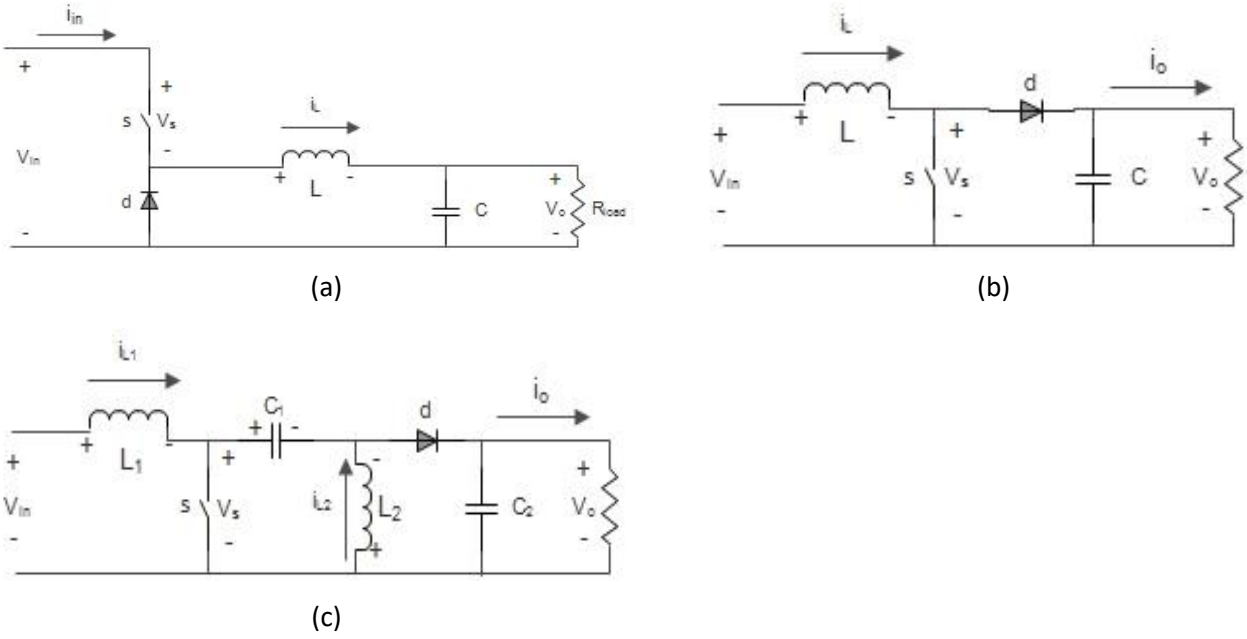

Figure 8: DC-Converters electrical configuration (a) Ideal Buck Converter, (b) Ideal Boost Converter, (c) Ideal SEPIC converter.

The sources of power losses in these converters comes from the passive elements such as the load, capacitor and inductor; and from the switching elements. The losses from the passive elements can be modeled and estimated. However, for the switching elements, many factors come into place. Such as the type and model of the switch, the switching frequency, the type of DC converter, the voltage applied at the switch gate, the gate capacitance and others.

In general, all types of switches follow the same two equations. Equation (2.7) occurs when there is a transition between the OFF-ON or the ON-OFF states of the switch, so it is called the switching losses equation. Equation (2.8) occurs when the switch is turned on and experiencing joule heating from the current passing through, so it is called the conduction loss equation.

$$P_{sw} = \frac{1}{2} V_{in} I_o f_s (t_{on} + t_{off}) \tag{2.7}$$

$$P_{cond} = I^2 R_{int} \tag{2.8}$$

Where V_{in} is the input voltage to the switch, $I_o$is the current output, f_s is the switching frequency, t_{on} and t_{off} are the rise and fall times and R_{int} is the switch internal resistance.

To calculate the rise time and fall time for equation (2.7) of the switch is not simple as it depends on the manufacturing of that switch. There are accurate models that can be found in recent SPICE simulators or from manufacturers specifications. However, these models are intended to work in a time scale of micro/milli- seconds at most, trying to run these models in larger periods proves to be very slow. They are not suitable for simulation such as in this work where the time scale is in hours.

In literature, a study by Munk-Nielsen [23] shows that combining ideal modeling of the switch with measured values of the losses in the form of a look- up table provides good results when compared to experimental values. Which provides a significant decrease in the simulation time specially for large number of switches.

Drofenik [24] showed that there are generally two ways to model switched for high speed simulations, it is by using experimental data or data sheet values alongside an ideal model for the switch without sacrificing accuracy he also described how to apply or fit the measured and data sheet values into the power loss equations.

Other studies [25], [26] also seem to use the described methods to model faster switches. In this study, the switch parameters will be determined using datasheet values. A power loss model based on these parameters is implemented. Finally, using this model in all the DC- converter configurations discussed, the power loss on each DC- converter can be investigated.

2.5. Energy Storage System

An Energy Storage System (ESS) is a fundamental block for islanded DC- micro-grids. As it allows the grid to become more flexible by managing the energy flow from the power generators to the loads. There are various technologies used for ESS where each has its unique characteristics and applications, some examples are: super capacitors, batteries and flywheels. The difference between these technologies are the Power Density (W/kg), Energy Density(Wh/kg), life cycles and cost.

Table (2) [27] shows some of the technologies for the electrical ESS and compares their main characteristics by showing some common values. Based on this comparison it is clear that each technology was designed for specific kind of applications. Super capacitors for example are used in applications that deal with a lot of transients due to their long-life cycles and power density. Same goes for the flywheels. Batteries on the other hand have relatively shorter life cycles and power densities and have higher energy densities and low specific energy cost which makes them more suitable for applications with steady operation and high energy storage demands. Usually combinations of ESS technologies are used for applications that require both high energy demands and power transients.

Table 2: Major Characteristics of Energy Storage Systems [27].

	Lead- Acid	**Li-ion**	**Super- capacitor**	**Flywheel**
Power Density (W/kg)	1000	1500	10,000	1000
Energy Density (Wh/kg)	40	150	10	0.3
Power Efficiency (%)	70-85	92-98	85-98	90-95
Cycle Life (cycles)	1000	1900	>50,000	>50,000
Internal Resistance (mΩ)	4	8	0.2	N/A
Specific Energy Cost ($/kWh)	120	600	5000	300

The most widely used battery chemistries in ESS are the Lead-Acid and Li-ion. Lead-acid is used mostly due to its acceptable performance and its ability to handle most WHR application transients at low cost as well as its recyclability [28]. Li-ion batteries on the other hand have higher power, energy densities and lifecycles. They are used in many applications such as automotive and portable electronics. However, the initial and replacement cost of Li-ion batteries is considered high for cost sensitive applications such as WHR systems [3]. For this reason, the Lead-acid chemistry is used for this study.

2.5.1. Battery Sizing

To size a battery for the DC micro-grid the IEEE standard 485-2010 [29] is used. The first step in sizing the battery is classifying the type of loads, which is divided into three categories: Continuous, non- continuous and momentary loads. Each type of load requires a certain discharge rate and capacity. In TEG POWER most electrical loads fall under the continuous category as they need to be powered for a long period of time if not always. Except for some momentary loads such as relays or valves. The sizing of the battery is thus determined by the continuous load demand.

The next step in the standard is to estimate a duty cycle or a load profile for your system to get an estimation for the required energy and power demand of the load. For this study a general load profile for a restaurant is assumed. This profile is based on the time of day, the popularity time and the necessary loads. For waste heat recovery power sources the profile also needs to be determined as they are not constant. The TEG system daily temperature profile is assumed based on how the ovens operate in such systems [30], the model in [6] emulating the heat exchanger and TEG system of the second generation TEG POWER is used to determine the TEG system output power.

Here an issue arises for islanded DC micro-grids, the total daily energy sum of the load profile for such system needs to be the same as the power source which is the TEG system. Without this balance the battery will either discharge overtime if there is a high load demand or overcharge in the opposite case when the power source is providing more power. This is practically

impossible to achieve. As a result, the loads and the power source need to be controlled. This is achieved by using load shedding and controlling the battery and MPPT systems.

The last step to size a battery is to calculate the capacity of the based on the load duty cycle. The following equation is used to determine the battery capacity.

$$c = \frac{\sum_{P=1}^{P=s} E_P}{V_B} \tag{2.9}$$

Where c is the battery capacity, E_P is the required energy per a period, it can be calculated by subtracting the load demand from the energy provided by the TEG system. P is the period of each step in the load profile (1 hr.) and V_B is the nominal battery voltage, in this project a 12V battery is used for the DC micro-grid.

Another factor discussed in the IEEE standard was aging which degrades the performance of the battery. Aging occurs by many factors such as the battery life cycle and the operating conditions such as temperature and the Depth of Discharge (DOD) which is the State of charge lower limit value [31] [32].

Depth of Discharge is one of the main operating conditions that must be considered when sizing a battery for ESS. A study by UweSauer [33] shows different factors affecting the age of the battery. The effect of DOD was summarized in table (3). The lifetime is defined by a Depth of Discharge (DOD) of 80%, when the battery is discharged for example with a DOD between 80% to 100% the life time is estimated at 68% of the original lifetime. The opposite is true as well, when the battery is cycled at a lower DOD the lifetime is improved, which means that when designing the battery storage for the DC-micro-grid, it is important to avoid cycling at a high DOD value specially for WHR applications where lifetime is an important factor. This is done by assuming a maximum DOD when calculating the battery capacity and preventing discharge beyond this value. The effects of DOD can be shown from Table (3).

*Table 3: The effect of STATE OF CHARGE LIMIT for discharge rates between 0.5*c *and 1*c on the battery life cycle [33].

Lead- acid battery charging condition	$\frac{Life\ Cycle}{Life\ Cycle_{DOD\ 60\%-80\%}}$
Max. STATE OF CHARGE LIMIT 0 − 10% followed immediately by a full recharge	887%
Max. STATE OF CHARGE LIMIT 0 − 20% followed immediately by a full recharge	452%
Max. STATE OF CHARGE LIMIT 20 − 40% followed immediately by a full recharge	247%
Max. STATE OF CHARGE LIMIT 40 − 60% followed immediately by a full recharge	157%
Max. STATE OF CHARGE LIMIT 60 − 80% followed immediately by a full recharge	100%
Max. STATE OF CHARGE LIMIT 80 − 100% followed immediately by a full recharge	68%
STATE OF CHARGE LIMIT 100% followed by a waiting period of up to 24 h before a full recharge is started	58%
STATE OF CHARGE LIMIT 100% followed by a further discharge with approximately 0.005C for up to 24h followed by a full recharge	37%

The equation for calculating the battery capacity when preventing the battery from surpassing a STATE OF CHARGE LIMIT shown in equation (2.10). The required battery capacity is increased by the $DOD\%$ threshold determined by the user:

$$c = \frac{\sum_{P=1}^{P=s} E_P}{V_B} * DOD\% \tag{2.10}$$

One additional effect that needs to be considered is the charge rate of the battery. As it effects the capacity of the battery. The battery charge rate is usually denoted by factors multiplied by the capacity, for example charging a battery with 1C means that a battery will take one hour to recharge from empty to full.

The battery responds differently with each value of a charge rate applied. The actual battery capacity changes from its nominal value as the actual battery capacity is a function of the charge rate. This is the reason why most battery manufacturers will state that the nominal capacity of a battery is when it operates at a standard rate of 0.2C or fully discharging a battery over a 10h period. This phenomenon was first described by Peukert's law [34]:

$$c_a = c(\frac{I_n}{I_a})^{pc-1} \tag{2.11}$$

Where I_n is the batteries nominal current, I_a is the actual current, c_a is the actual battery capacity, and pc is Peukert's coefficient. Peukert found that pc is approximately 1.47 for lead-acid batteries. However, new lead-acid batteries will have a smaller value because the improvement in battery design and technology.

Based on Peukert's law, if the battery is discharged with a higher current value than the nominal, it will have a lower actual capacity and if the actual current is smaller than the nominal, the actual capacity will be greater than the nominal capacity.

To maximize the energy utilized by a battery, it is important to choose the appropriate capacity c in such a way that the actual current values needed during operation are smaller or equal to the nominal current and limit the battery current to not exceed it as much as possible.

2.6. Energy Management System

An Energy Management System (EMS) is used in DC-Micro-grids for several reasons: to maintain the battery State of Charge (SOC) at a certain range, protect the battery from over charging and under charging and to maintain the power balance between the power source, load and battery.

In literature numerous EMSs have been developed. In [10] an EMS was developed switch the operation of a micro-grid from utility connected to islanded mode in case of power fault. A study by Zhang, Y. [35] shows EMS for PV array and wind turbine systems which can be used in remote areas where micro-grids are islanded from the utility grids. The EMS in this study had three main functions: prevent the battery from surpassing certain SOC values, preventing over charge/ discharge power on the battery and load shedding in case of low power output.

For micro-grids connected to the utility grid, Luna, A [36], developed and tested an online EMS with the ability to predict, schedule and optimize a DC-micro-grid performance. An optimization case was designed and implemented that prioritizes minimizing the energy cost by utilizing the utility grid on at low cost hours while maintaining the operation of the grid. In [37] a EMS for a residential building was developed. The EMS can plan a day ahead for the energy demands of the system and buy/sell the energy to the utility grid based on the per hour price.

From Figure (1) in the beginning of this chapter, the loads in the DC micro-grid was divided according to their priority. Some loads were necessary to operate such as the components needed to run the DC micro-grid and the TEG POWER setup itself. The EMS for this micro-grid should be able to turn off loads in case of load shedding according to their priority. In this study, an EMS is designed for the islanded micro-grid. The EMS should be able to control the operation of the MPPT, battery system and loads to ensure maintenance of operation.

Chapter 3

DC-microgrid System Modeling

3.1. Introduction

In this chapter the numerical and analytical modelling of the different components of the DC-micro-grid is presented. Figure (9) shows the different components and how they are interconnected.

The integration of the TEG Heat exchanger numerical model (TEG/HX) is first discussed [6]. Followed by modeling of the DC converters with the analytical modeling of the electrical power losses, then the MPPT algorithm used and its appropriate parameters for operation and finally, the battery system along with the battery protection modes are discussed.

The model was developed in MATLAB Simulink using SimPower and State Flow toolboxes.

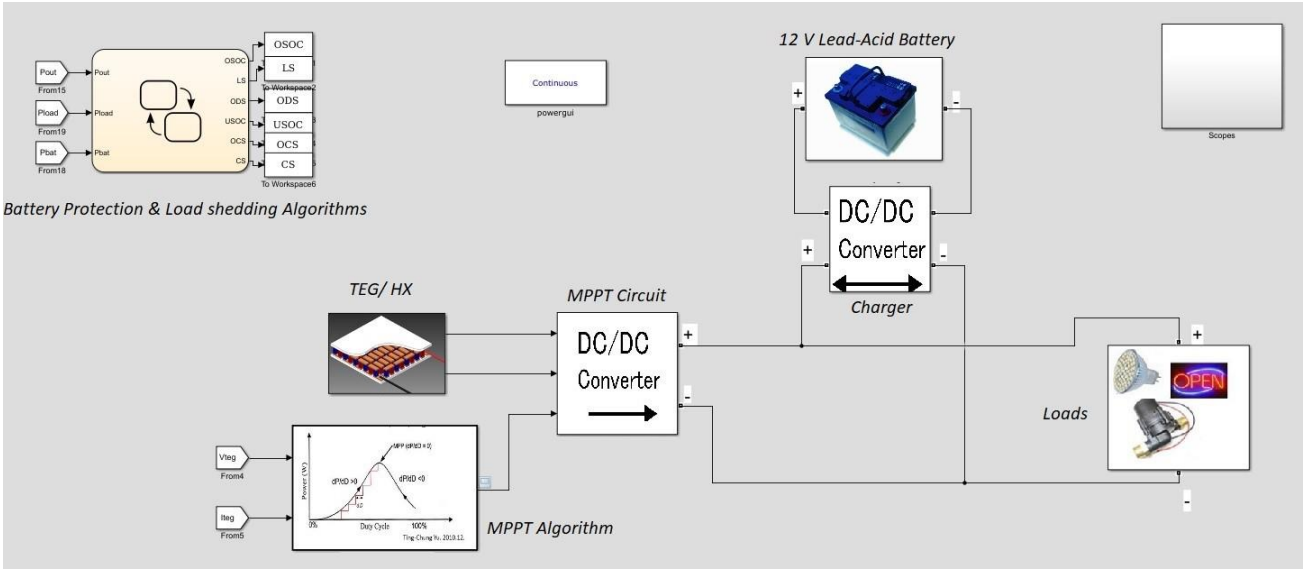

Figure 9: DC Micro-grid Simulink Model

3.2. TEG System

3.2.1. TEG/ Heat Exchanger Numerical Model

The TEG in a heat exchanger model studied by Zaher [6] was used as the input to the system. The model can simulate the performance of the TEGs under different series or parallel electrical configurations. Figure (10) shows the thermal network of a TEG operating in a heat exchanger under a hot side temperature $T_{T,H}$ and a cold side temperature $T_{T,C}$. with a thermal resistance $R_{th,TEG}$ and an electrical resistance r_{TEG}. For the heat exchanger, the hot side is the exhaust gas side with a thermal resistance $R_{th,H}$, inlet and outlet exhaust gas temperatures of $T_{g,in}$, $T_{g,out}$ and exhaust gas mass flow rate $\dot{m}_{gas}$. The cold side is the water side, with thermal resistance $R_{th,C}$ with inlet and outlet temperatures $T_{w,in}$, $T_{w,out}$ and water mass flow rate $\dot{m}_{water}$. $R_{th,A}$ is the axial conduction resistance between the TEG rows and $R_{th,G}$ is the gap thermal resistance due to spacing between TEGs. Figure (11) shows the TEG rows connected thermally and electrically, for all the rows.

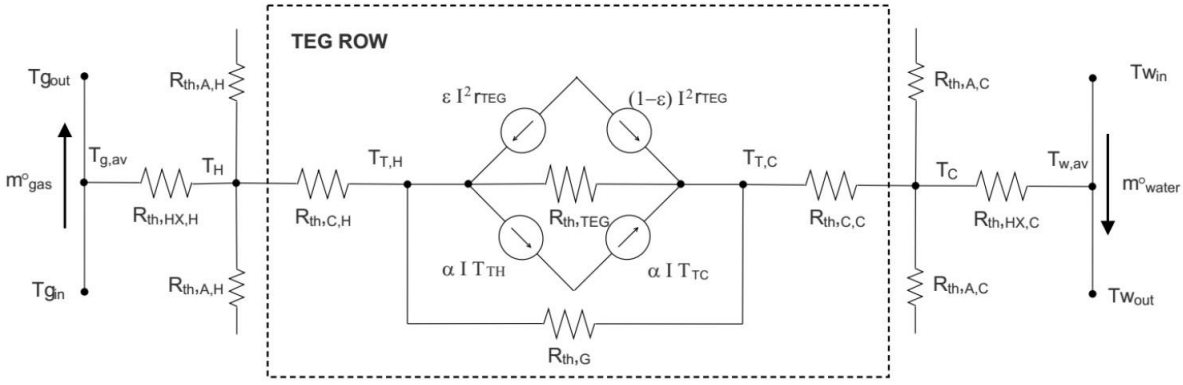

Figure 10:Thermal network for a TEG row including thermal contact resistances in a heat exchanger and axial conduction between rows [6].

The governing equations in the model solves iteratively for the heat exchanger. $\dot{m}_{water}$ and $\dot{m}_{gas}$ are obtained using solutions of previous iterations for temperature after their initialization. The other parameters are set as initial conditions for the system.

For the electrical output, the solution is dependent on the electrical connection of the TEG rows in series or parallel. Once the thermal solution is obtained the electrical solution is estimated from each TEG row, where voltage and current output are estimated. The initial conditions required by the model is the initial gas temperature at its inlet, the water temperature, the gas mass flow rate and the water mass flow rate.

The model can simulate different TEG configurations where the number of rows is predetermined along with the connection between them in series or parallel.

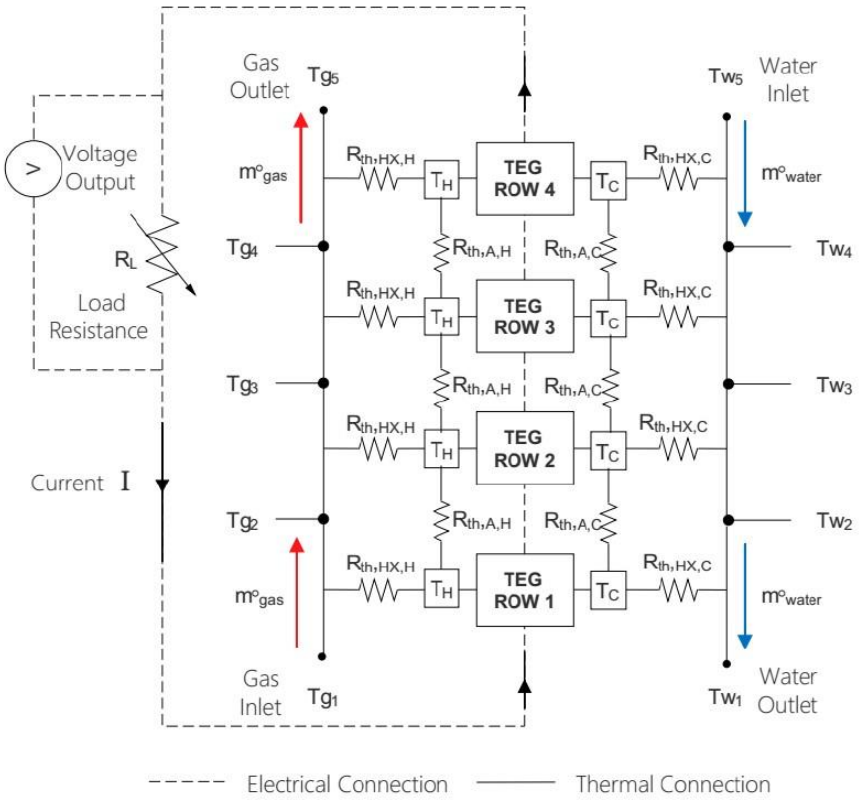

Figure 11:Thermal network for a multi-row heat exchanger with integrated TEGs including the electrical connection circuit between TEG rows [6].

3.2.2. TEG Equivalent Circuit Representation

For electrical systems a TEG can be modeled using an equivalent circuit consisting of a controlled voltage source and a variable resistor connected in series as shown in Figure (12). The

controlled voltage source models the open circuit voltage V_{OC} of the TEG while the variable resistor models the internal resistance R_{TEG}.

Assuming the circuit is connected to a load resistor R_{Load} at its terminal end and applying Kirchoff's law.

$$V_{OC} = V_{TEG} + V_{Load} = I(R_{TEG} + R_{Load}) \tag{3.1}$$

$$I_{TEG} = \frac{V_{OC}}{(R_{TEG}+R_{Load})} \tag{3.2}$$

$$P_{Load} = V_{Load}I_{TEG} = I_{TEG}^2 R_{Load} = R_{Load}\frac{V_{OC}^2}{(R_{TEG}+R_{Load})^2} \tag{3.3}$$

Plotting the power relation with V_{TEG} will result in the P-V curve for the TEG and plotting the V_{TEG} with I_{TEG} will result in the V-I TEG characteristic curve. It shows that the maximum power condition is achieved when $R_{Load} = R_{TEG}$ which agrees with the TEG characteristics discussed in section 2.4.

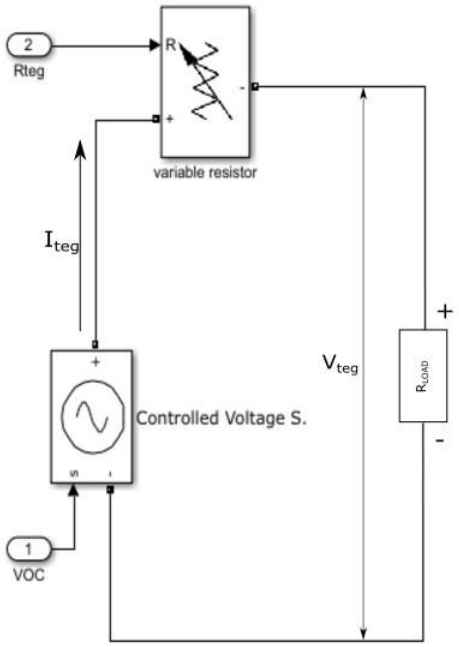

Figure 12:TEG Electrical Equivalent Model in Simulink.

3.3. Power Loss Analytical Model

This section discusses the power losses from the DC converter circuit for the MPPT as this part of the circuit is affected by the TEG configuration.

This model is designed to input the parameter values of a real MOSFET from its manufacturers data sheet. The procedure use Graovac and Prschel [38] is used to calculate the values required to determine the power losses for the MOSFET.

As shown in Figure (13), two ideal MOSFETS representing a part of a half bridge which is commonly used for most synchronous DC converters are connected to the loss model. Beginning from the left side of the Figure the first block separates the MOSFET forward bias and reverse bias measurements. The forward bias represents the main MOSFET while the reverse bias represents the freewheeling diode.

After the measurements are separated it is connected to two main blocks, one block is responsible for calculating the losses due to switching while the other is for calculating the conduction losses.

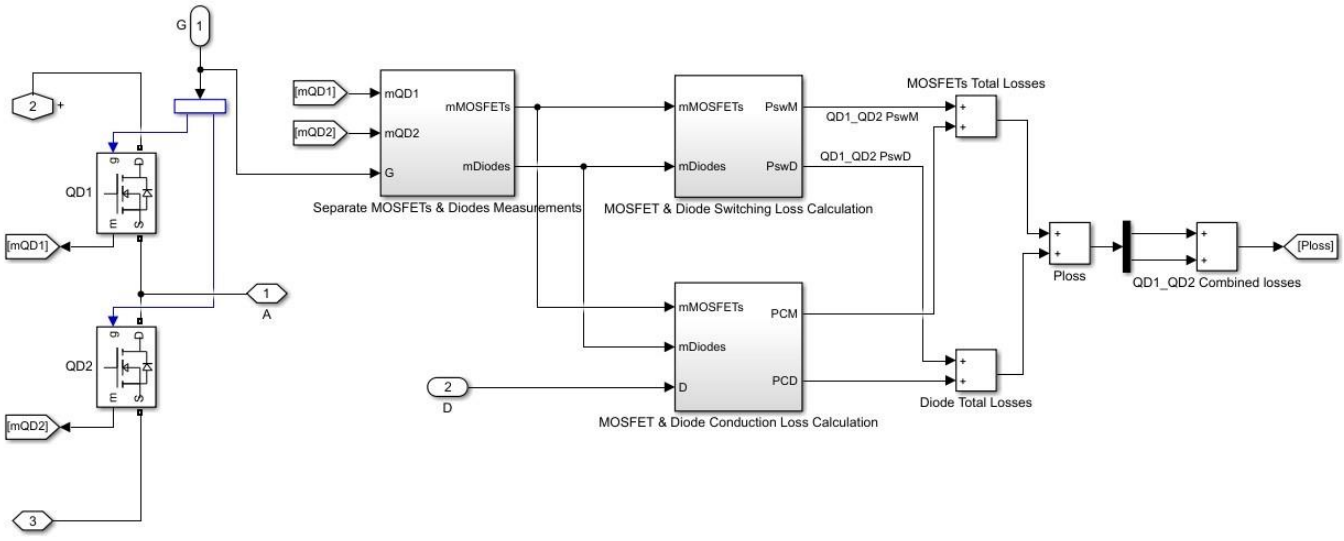

Figure 13: Simulink Power Loss Model for The MOSFET Switches

Figure (14) shows the subsystem for the block responsible for the switching losses while Figure (15) shows the subsystem for the block responsible for the conduction losses.

The switching losses model in Figure (14) is based on the equations discussed in section 2.4., the blocks referred as EON MOSFET and EOFF MOSFET includes the energy equations 2.26 and 2.27 with a minor difference for EON MOSFET to include the effect of the reverse recovery of the freewheeling diode such that [38].

$$E_{M(on)} = \frac{1}{2} V_{in} I_o \left(t_{ri} + t_{fv}\right) + Q_{rr} V_{in} \tag{3.4}$$

Where Q_{rr} is the reverse recovery charge measured in nano Columbs *nC*. The bottom part is for the diode turn on energy due to reverse recovery.

$$E_{d(on)} = Q_{rr} V_d \tag{3.5}$$

Where V_d is the voltage across the diode during reverse recovery.

After the energy losses are calculated they are multiplied by the switching frequency f_s which results in the power loss per switching period. The value of this power is held throughout the switching period so that the model gives a continuous result.

The conduction power losses in Figure (15), consists of two equations: First for the MOSFET conduction.

$$P_{CM} = I_{on,rms}^2 R_{DS} \tag{3.6}$$

Where R_{DS} is the Drain Source resistance or the resistance when the MOSFET is switched on. The Second part is the diode conduction losses.

$$P_{CD} = I_{f,rms}^2 R_D + I_f V_f \tag{3.7}$$

Where R_D is the diode resistance, I_f is the current passing through the diode and V_f is the diode forward voltage.

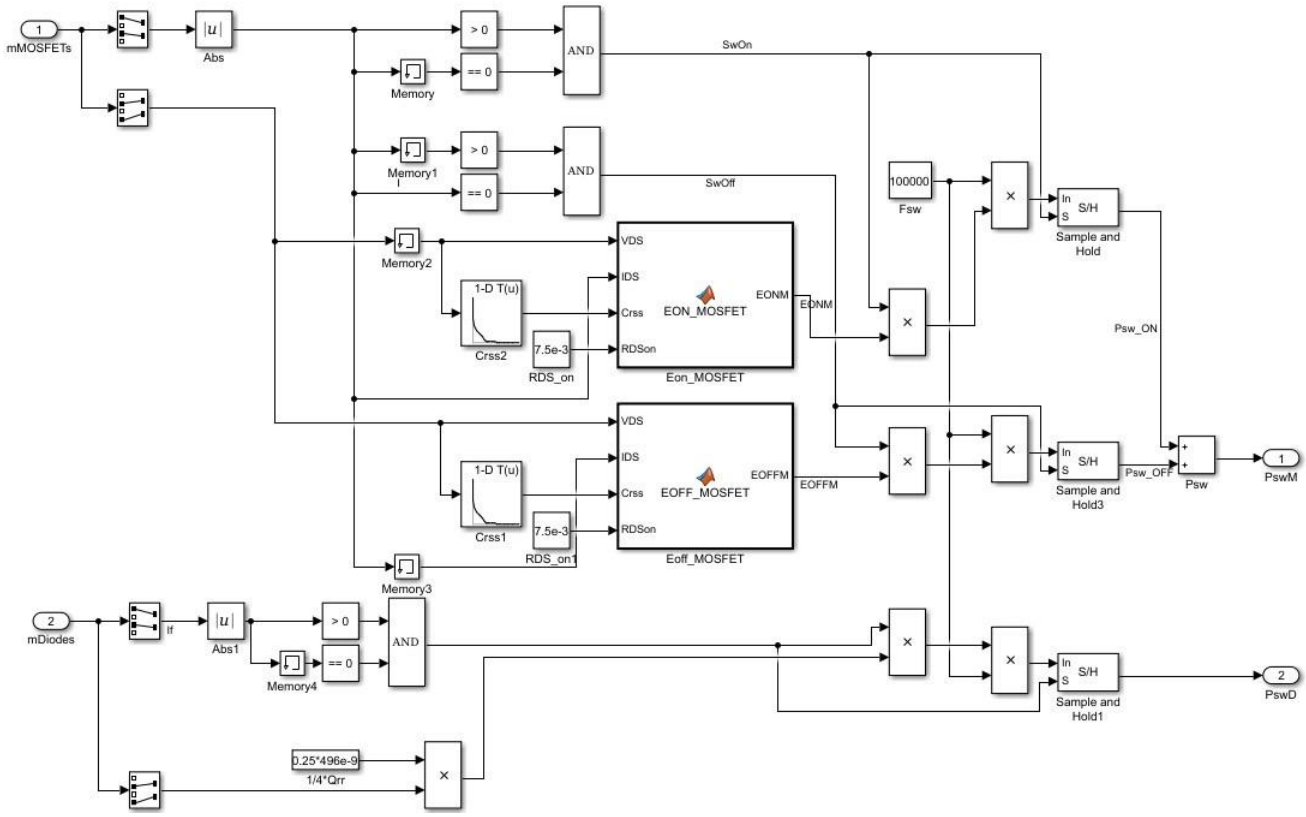

Figure 14:Switching Losses Calculation for the MOSFETS

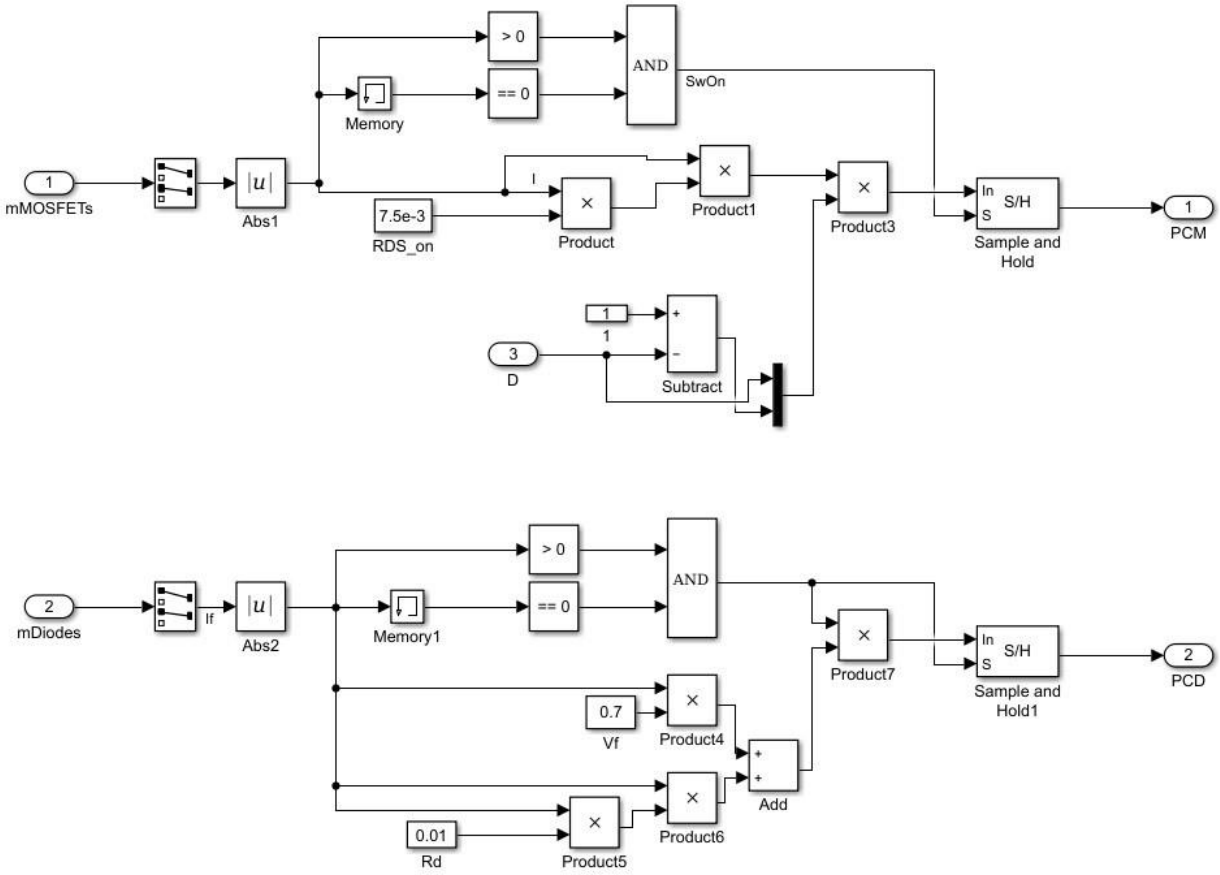

Figure 15: Conduction Losses Calculation for the MOSFETS

3.4. DC Converter Circuit numerical model

This section shows the integration of the power loss model and the TEG equivalent circuit into different DC converters used for the MPPT or the battery charger. For each converter topology the switch interconnections could be slightly different than what was shown in Figure (13) due to the nature of the DC converter configuration which was taken into consideration while modeling.

Figures (16) to (19) show the model for each of the converters used in this study. The switches and the power loss model were combined into one subsystem called Half Bridge MOSFETs. For the Buck, Boost and SEPIC converters the equivalent TEG circuit is connected at the input.

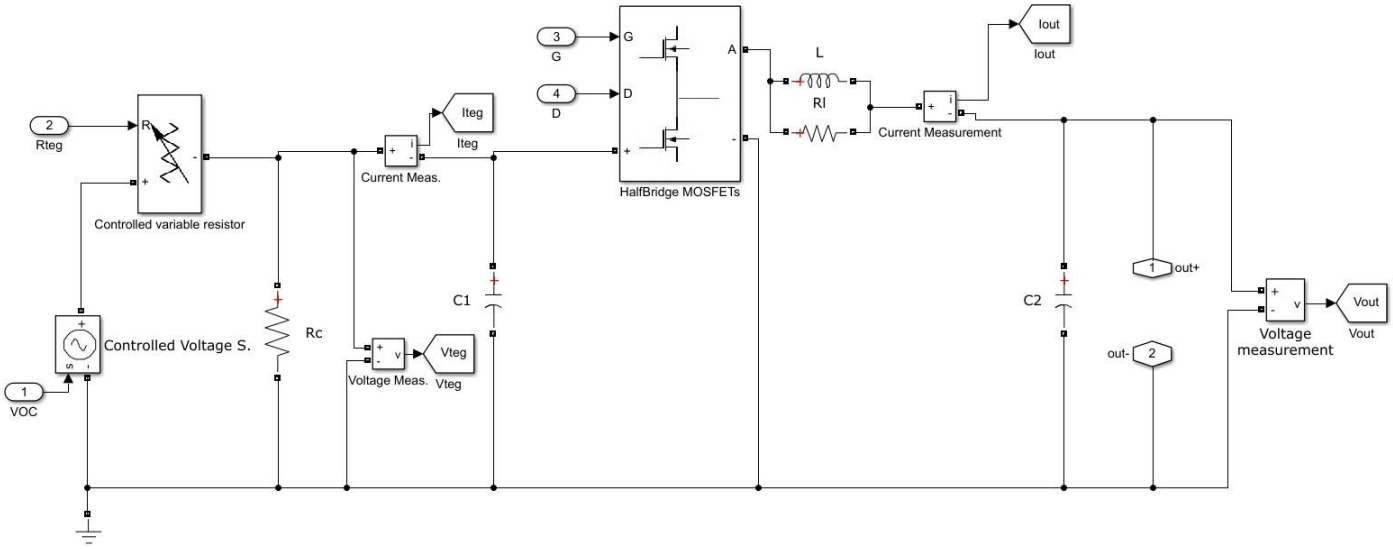

Figure 16:Buck Converter with MOSFET Power Loss Model

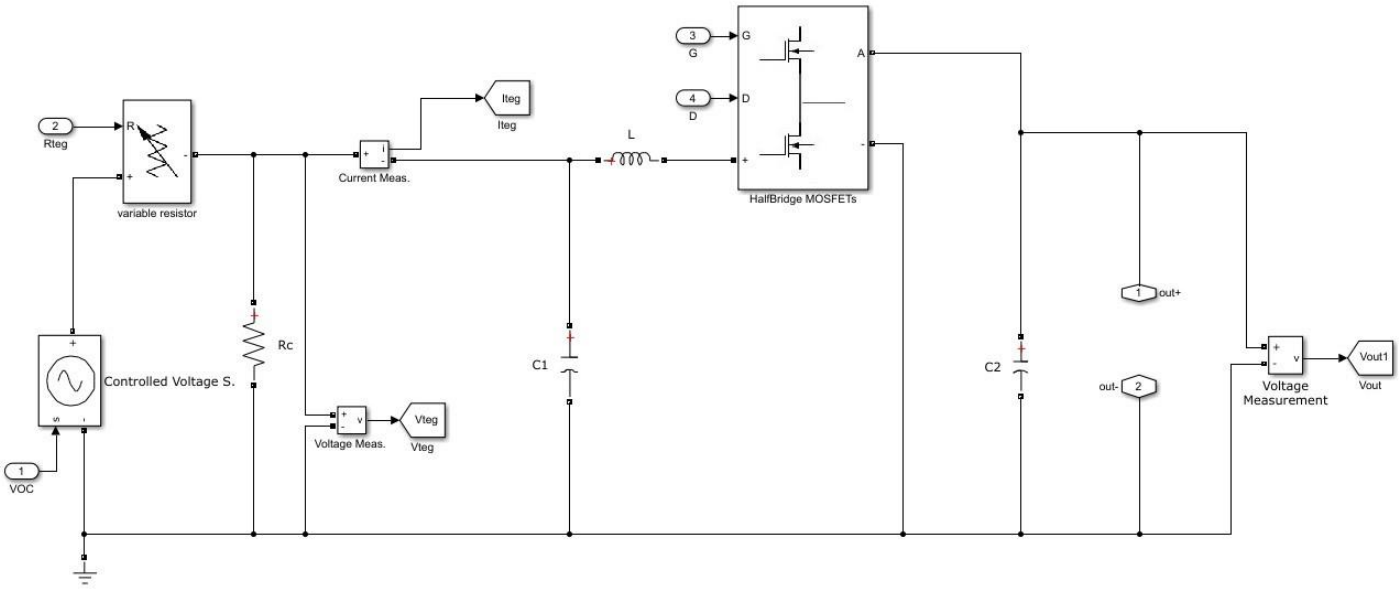

Figure 17:Boost Converter with MOSFET Power Loss Model

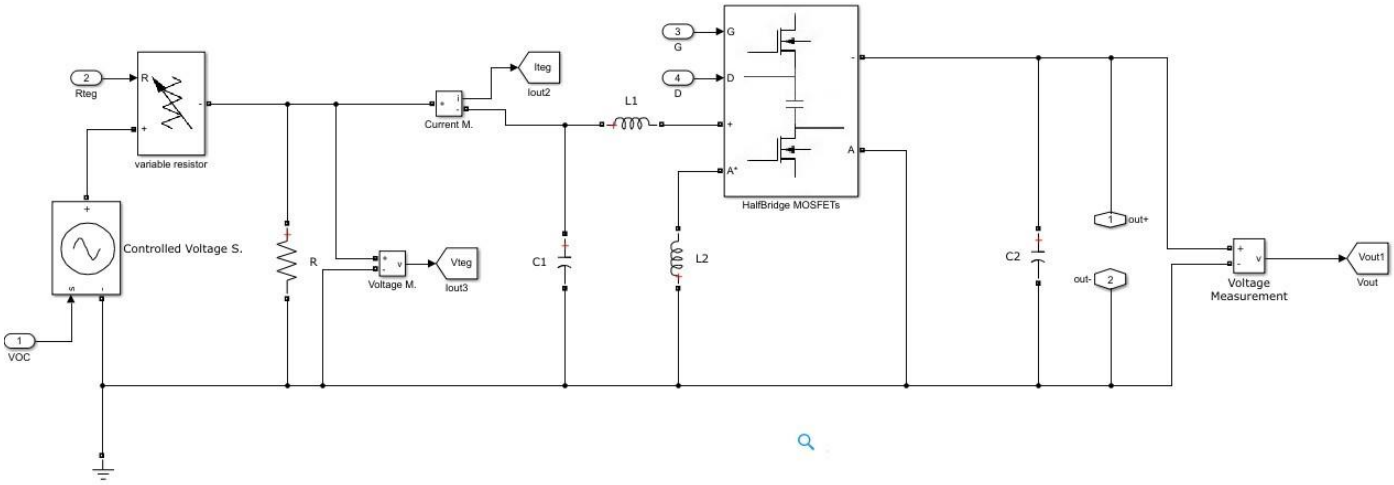

Figure 18: SEPIC Converter with MOSFET Power Loss Model

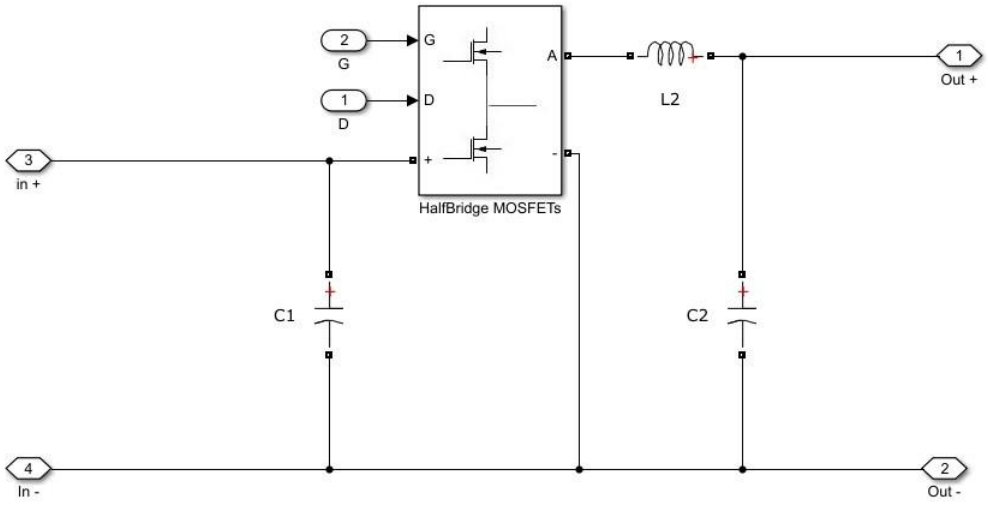

Figure 19: Bidirectional Buck Boost Converter with MOSFET Power Loss Model

3.4.1. Components Sizing

The DC converters for the MPPT are connected to the TEG array on the input side and connected to the 12*V* load and battery side at the output. The main objective of sizing the converter components are to always operate at Continuous Conduction Mode (CCM) and to maintain a smooth voltage and current wave forms at both the input and output to minimize any power losses.

The TEG array is assumed to operate at a constant power value which is the maximum power point where the components are sized accordingly. The input voltage and current for the converters in this case will be half the V_{OC} and I_{SC} values. There are three levels of input power being studied: 100W, 200W and 300W. At each level the circuits are designed according to the value for the components. The sizing of the capacitors and inductors are achieved using the equations shown in Table (4) they ensure the output voltage and current ripples remain under a value of 5% to avoid power losses the equations intrinsically insure Continuous conduction mode CCM operation as well. The values for the components are shown in Table (5).

Table 4: Sizing of DC Converter Components [22].

Buck	$L = \frac{V_{out}^2(1-D)}{PI_{percent}f_s}$	$C = \frac{(1-D)}{8Lf_s^2V_{percent}}$
Boost		$C = \frac{2V_{out}^2D}{PV_{percent}f_s}$
SEPIC	$L = \frac{V_{in}D}{I_{percent}I_{in}f_s}$ $L = \frac{V_{out}^2(1-D)^2}{PI_{percent}f_s}$ $L = \frac{V_{out}^2(1-D)^2}{PI_{percent}f_s}$	$C = \frac{(I_{Lmax}-Iout)^2(1-D)}{V_{percent}2I_{percent}(I_{in}+I_{out})f_sV_{out}}$
Bi. Buck-Boost		$C = \frac{(I_{Lmax}-Iout)^2(1-D)}{V_{percent}2I_{percent}(I_{in}+I_{out})f_sV_{out}}$

Table 5: Components Values at Different Power Levels

Topology	*P* = 100*W*		*P* = 200*W*		*P* = 300*W*	
Buck	$L_{0.1}$ = 259.3*μH*	$C_{0.1}$ = 868.1*nF*	$L_{0.1}$ = 129.6*μH*	$C_{0.}$1 = 1.736*μF*	$L_{0.1}$ = 86.4*μH*	$C_{0.1}$ = 2.604*μF*
Boost	$L_{0.8}$ = 0.46*μH*	$C_{0.8}$ = 230*μF*	$L_{0.8}$ = 0.24*μH*	$C_{0.8}$ = 115*μF*	$L_{0.8}$ = 0.154*μH*	$C_{0.8}$ = 76.8*μF*
SEPIC	$L_{0.1}$ = 0.233*mH*	$C_{0.8}$ = 570*μF*	$L_{0.1}$ = 0.117*mH*	$C_{0.8}$ = 380*μF*	$L_{0.1}$ = 0.078*mH*	$C_{0.8}$ = 190*μF*
Bi. Buck-Boost	N/A		$L_{0.4}$ = 51*μH*	$C_{0.6}$ = 220*μF*	N/A	

3.5. MPPT Algorithm

The MPPT P&O algorithm implemented was discussed in section 2.3., using a MATLAB script. The MPPT however changes the duty ratio directly instead of changing the reference voltage value of a controller. This algorithm was chosen because of the case studied in this work is slow compared to other dynamic systems, the P&O algorithm is more than capable of tracking the maximum power point for this system. The sampling rate was chosen to be $\tau_s = 0.001sec$. Each sample the MPPT algorithm will change the duty ratio of the DC converter with a step size of $\Delta d = 0.001$. The initial duty ratio was set at $D = 0.5$. In this case, the worst-case scenario for tracking a value would be reaching $D = 0$ or $D = 1$, it would take a tracking time of $0.5sec.$, which is suitable for our system. A similar real thermal system would usually take more time compared to the MPPT algorithm due to the thermal capacitance [30].

The MPPT algorithm was also designed to track other points on the P-V curve away from the maximum power in case of other modes of operation where maximum power point tracking would damage the battery or the loads, this part is discussed in detail in Section 3.7.

Figure (20) shows the electrical characteristics of the MPPT tracking a TEG/HX system with a maximum power point $P_{max} = 200\ W$ Where V_{teg} is the input voltage to the MPPT, V_{out} is the output voltage, I_{teg} and I_{out} are the input and output currents; and P_{teg} and P_{out} are the input and output power. The algorithm was connected to a buck converter for this simulation and it was able to step down the TEG voltage at steady state from $80V$ down to $12V$. The $12V$ at the output of the MPPT circuit was held at this value by the battery system. The output power P_{out} of the MPPT is less than the TEG power P_{teg} due to the electrical losses from the switching and parasitic components.

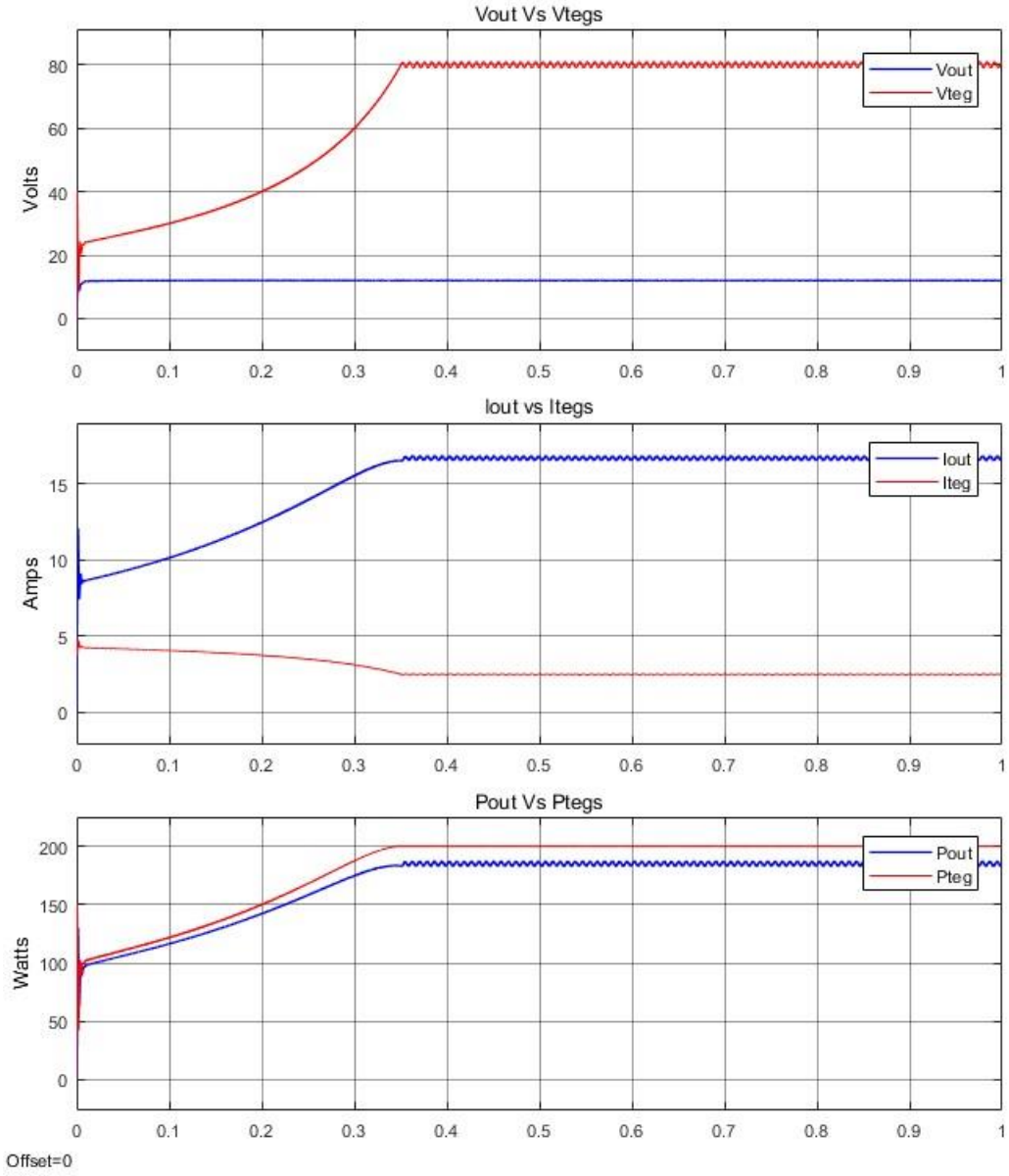

Figure 20: MPPT tracking at $P_{TEGmax} = 200$W, $\Delta\delta_B = 0.001$, $\tau_s = 0.001$sec

3.6. Battery System numerical model

The battery system mainly consists of three parts the bi-direction buck boost converter modeled in section 3.4, the control system and the battery itself.

The main function of the battery system is to compensate for the mismatch between the TEG power source and the load demand in case the TEG system is unable to provide enough power, or to store the excess energy in case the TEG system is generating more power than the demand. Another important task for the battery system is to maintain a constant voltage at the load side of the electrical system, $12V$ in this case.

The control system is simply a PI controller, which has the load voltage measurement as an input and has a reference voltage value of $12V$. Depending on the measured load voltage the PI controller will adjust the duty ratio D of the bi-directional buck boost converter so that the power going through it would be able to maintain the system at the reference voltage.

However, the issue with the whole DC micro-grid system model at this stage is the slow simulation time. For example, the electrical models in the MPPT and battery charger simulation times are in order of milliseconds of simulation time (i.e. every 100 milliseconds are equivalent to 5 seconds in real time) while the battery system charge requires a few minutes/ hours of simulation time to have a significant change. For this reason, it would be appropriate to separate the model into two parts, the first is responsible to run the electrical system up to steady state and the other part is responsible to charge the battery separately from the electrical model (as the battery model would solve faster when it's separated from the electrical model). The electrical model in this scenario only needs to run until steady state only and then it passes all the required data to the separate battery model to run. By using this method, the simulation would solve faster than using only one combined model and several case studies could be tested as will be shown later in the results chapter.

Figure (21) shows a simple model of a current source connected to a battery, this model is used alongside the main model as discussed earlier. Once the system reaches a steady state on

the main model the battery power value is passed to this model as a reference value for the PI controller, the current source as a result will charge the battery with the same power value.

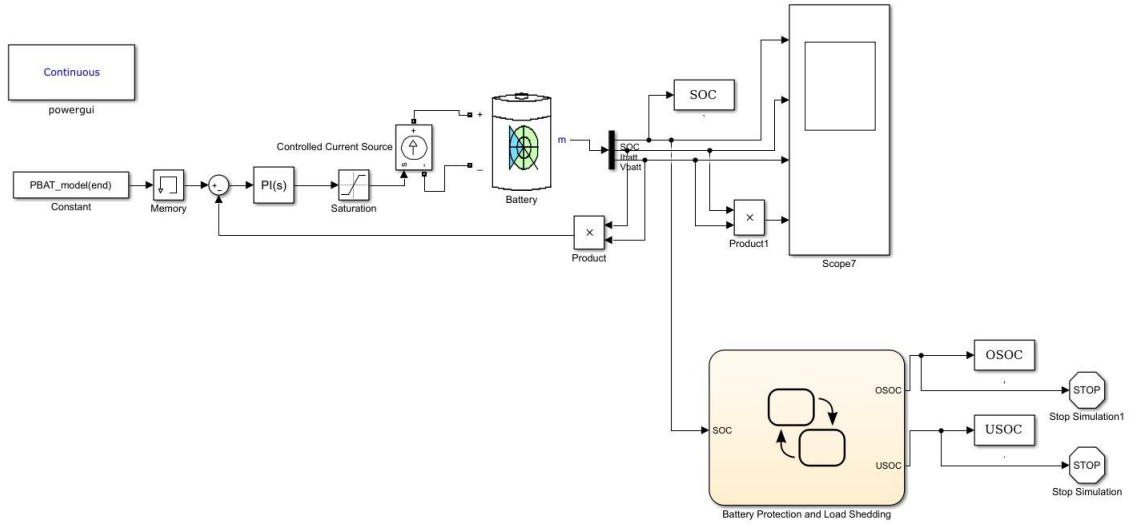

Figure 21: Battery charging model used for improving simulation speed

3.7. Battery Protection and Load Shedding Algorithms

Depending on the system state during simulation, the model goes into different modes of operation to keep the system from failing and to protect the battery from aging.

To keep the system operating the balance between the input power from the TEG system, the power losses, the battery storage power and the load power demand must be always maintained.

$$P_{TEG} = P_{Load} + P_{Losses} + P_{Bat} \ , \qquad P_{out} = P_{Teg} - P_{Losses} \tag{3.8}$$

$$P_{Out} = P_{Load} + P_{Bat} \tag{3.9}$$

Considering the power values change during operation, a control system is needed to ensure the power balance at all scenarios or the electrical system will fail. One case where the

maximum power is sacrificed is in scenarios where the power generated is more than the load demand $P_{Out} > P_{Load}$ and the battery is fully charge $SOC > SOC_{max}$. In this condition the MPPT must shift its operation away from the Maximum Power Point to a value where $P_{Out} = P_{Load}$ and $P_{Bat} = 0$, this mode is called Over SOC Limit Mode.

Another possible case is when the TEG system is also generating more power than the load demand $P_{Out} > P_{Load}$ and a battery with a certain capacity c is being charged. The power being delivered to the battery however exceeds its threshold power such that $P_{th} = 0.2c * V_{Bat}$ where V_{Bat} is the battery operating voltage. As in the previous case, the MPPT will need to shift from the maximum power point to a lower power where $P_{Out} > P_{Load}$ and $P_{Bat} = -P_{th}$, this mode is called the Battery Over Charge Protection Mode.

In contrast to the Over SOC Limit Mode, is a case where the power generated by the TEGs is less than the load demands $P_{Out} < P_{Load}$ the battery in this case will discharge power to compensate for the low power output. However, if the SOC of the battery goes under a certain threshold, the control system must stop the battery from going below that threshold and keep $P_{Bat} = 0$ until it starts to recharge again. Load shedding will occur in this case to balance the system to a value where $P_{Out} = P_{Load}$, this mode is called Under SOC Limit Mode.

The last case is when the TEG power generated by the MPPT is less than the load demand $P_{Out} < P_{Load}$ and the power being delivered by the battery exceeds its threshold power in this case load shedding will occur to balance the system where $P_{Out} < P_{Load}$ and $P_{Bat} = P_{th}$, this mode is called the Battery Over Discharge Protection Mode.

The model checks the system power balance at each iteration and will activate each mode as needed, Figure (22) shows a flow chart of the modes discussed.

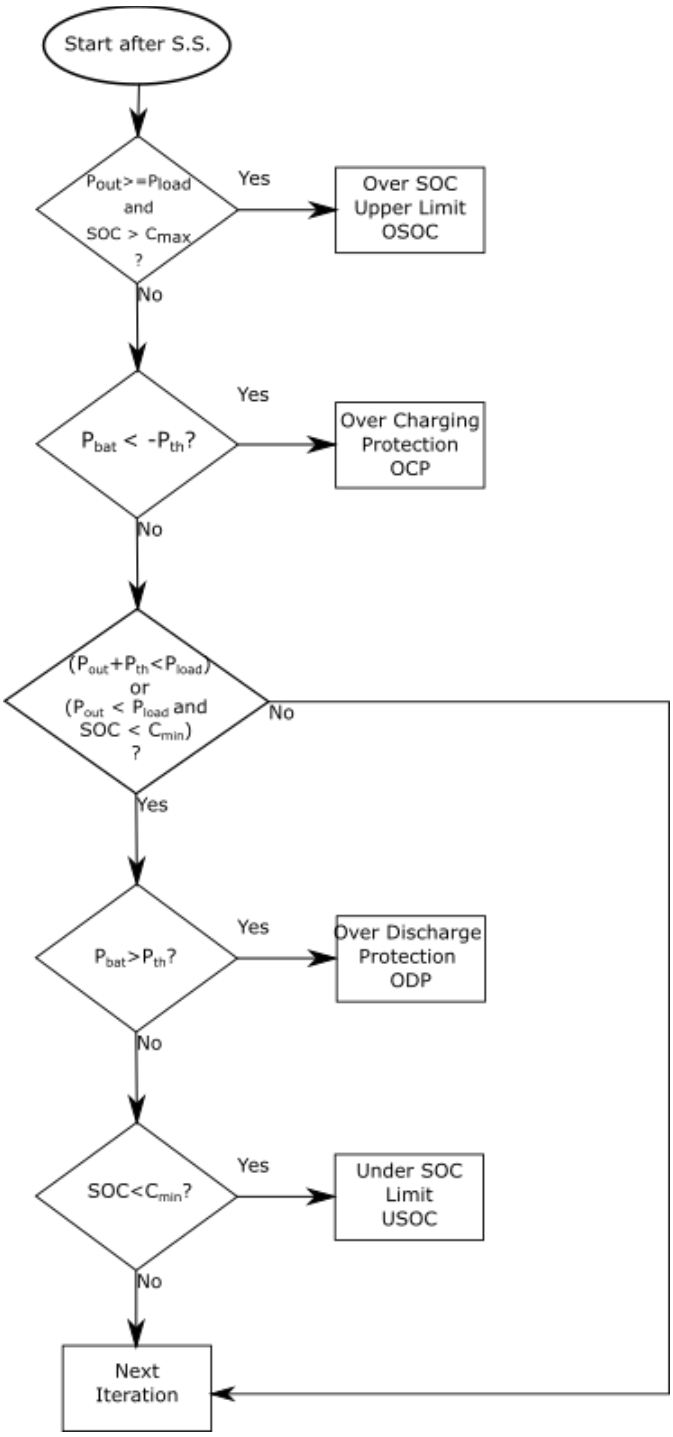

Figure 22:Battery Protection and Load Shedding Flow Chart

3.8. Model Solving Flow

The model starts by reading the input values for the TEG/HX model, the load profile and the initial conditions for the electrical system. It solves the TEG/HX model first and estimates the value of the TEG system parameters V_{OC} and R_{TEG} independent of the electrical circuit. The outputs of the TEG/HX model are used as the reference values for the TEG equivalent electrical model, V_{OC} is the input value to the voltage source and R_{TEG} is the input value to the variable resistor, the equivalent TEG model was explained earlier in Section 3.2.2.

The electrical model which includes the MPPT, the battery system and the loads solves and estimates the power values for the TEGs, MPPT output and the battery. It runs until the power balance is achieved at steady state. Then the model checks if one of the battery protection or load shedding conditions are triggered and adjusts the loads or the MPPT depending on which condition was activated.

The model then initiates the battery charging model explained in Section 3.6 using the value of the steady state battery power and the SOC of the battery. The battery charging model then solves and estimates the SOC of the battery during an hour of operation. If one of the battery protection modes for the over SOC or under SOC limits are activated, it stops the simulation and returns to the main electrical model readjusting the MPPT or initiates load shedding. The main model re-initiates the battery charging model again and continues to simulate the remaining time. After an hour is simulated the output power values and the SOC values are saved and a new iteration for the next hour starts with the SOC value from the previous hour and the new input values from the temperature and load profiles. The flow of the model is shown in Figure (23).

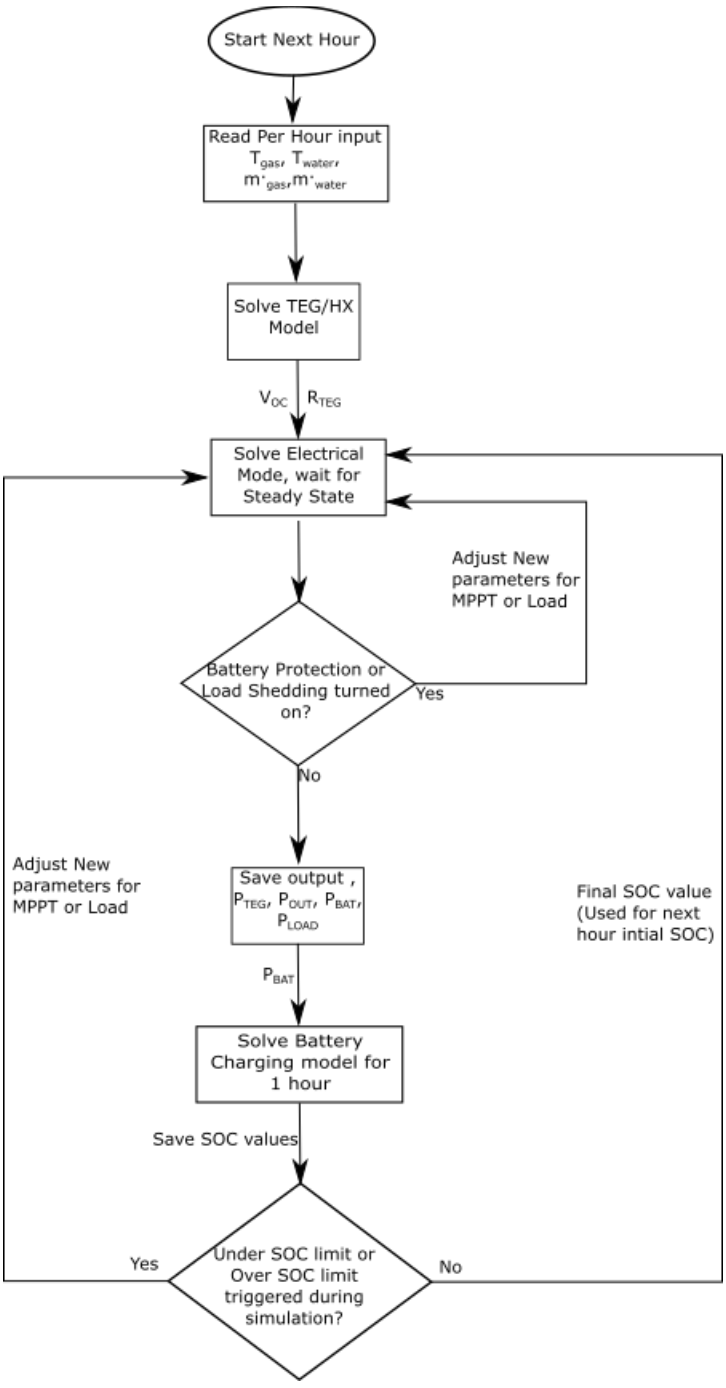

Figure 23: Model Per Hour Solving flow chart

3.9. Summary

Modeling the DC-micro-grid involves integrating the Thermal, logical and electrical systems together. The thermal model includes the TEG and heat exchanger and is solved using initial conditions for the temperatures and flow rates. The output from the thermal system are the TEGs electrical operating conditions which is interconnected to the electrical system involving the MPPT, battery and loads.

The MPPT model achieves the maximum power point, the tracking speed and fluctuations around the maximum power point were taken into consideration in the model. The battery is mainly used to manage the power of the system and limit the operation of the load at 12*V.* There are constrains for the battery and loads translated into modes of operation to stabilize and balance the system power. They are summarized as follows:

Table 6: Operating modes of the battery protection and load shedding control.

Modes	MPPT output vs. Load demand	Battery condition	Mode Target
Over SOC Limit Mode	$P_{Out} > P_{Load}$	$SOC > SOC_{max}$	$P_{Out} = P_{Load}$ and $P_{Bat} = 0$
Battery Over Charge Protection Mode	$P_{Out} > P_{Load}$	$\|P_{Bat}\| > \|P_{th}\|$	$P_{Bat} = -P_{th}$ (sign indicates charging)
Battery Over Discharge Protection Mode	$P_{Out} < P_{Load}$	$\|P_{Bat}\| > \|P_{th}\|$	$P_{Bat} = P_{th}$ and load shedding
Under SOC Limit Mode	$P_{Out} < P_{Load}$	$SOC < SOC_{max}$	$P_{Bat} = 0$ and load shedding

In the next chapter the losses of the electrical circuit are simulated and discussed as well as different case studies will be used to test the model and the DC micro-grid performance.

Chapter 4

System Losses, Case Study Analysis and Energy Utilized

4.1. Introduction

In this chapter power losses for different DC converters are shown under different power levels trying to simulate the fluctuating power levels of a TEG based power source. The DC converters tested are the buck, boost and SEPIC. The relation of the power losses for each converter in relation with the TEG configuration and the considerations required when choosing a DC converter for an application are discussed.

4.2. Converter Losses

4.2.1. Electrical Model Initial Conditions

The electrical losses mainly depend on the type of converter used either buck, boost or buck boost, the type of switches used, if the converter is synchronous or asynchronous, the power level, input and output voltages; and current levels. The simulations were made under the constraints and assumptions below:

- MOSFET switches are used as they are suitable for this range of Power [22]. The MOSFET *IPA*075*N*15*N*3*G* data sheet parameters are used in the loss model.
- The input and output power are equal, three values are simulated P = 100,200 and 300W.
- The output voltage is fixed at 12V which matches the required Load side operating voltage in the DC micro-grid.
- The input voltage is variable which simulates a TEG system with different configurations.
- The converters are operating in Continuous Conduction Mode (CCM).

4.2.2. Buck Converter Losses

In the case of a buck converter as in Figure (24), due to the inductor being placed on the output side of the half bridge. The inductor's current will always be equal to the output current and the sum of the switches currents is equal to the inductor current (See section 2.4.1). This means the conduction losses from the switches will be constant.

Considering equations 4.1 and 4.2 for the MOSFET energy losses and knowing that the rise and fall time are close values for most cases for these types of switches, approximating the first term for the total energy losses to be the input voltage multiplied by the output current or in this case the inductor current which is constant. It can be concluded that the switching losses is mainly dependent on the input voltage.

$$P_{CM} = I_{on,rms}^2 R_{DS} \tag{4.1}$$

$$P_{CD} = I_{f,rms}^2 R_D + I_f V_f \tag{4.2}$$

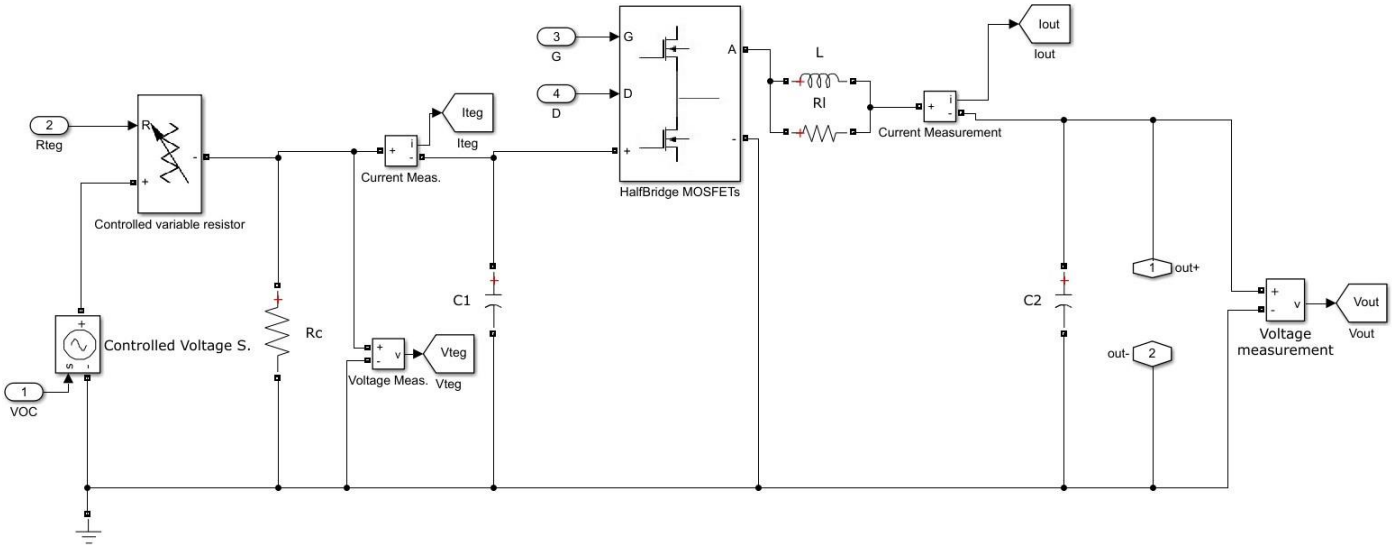

Figure 24:Buck Converter with MOSFET Power Loss Model

Figure (25) shows this relation. the conduction power loss in the switch and the inductor are constant through the whole OCV sweep. While the switching losses are increasing with the OCV.

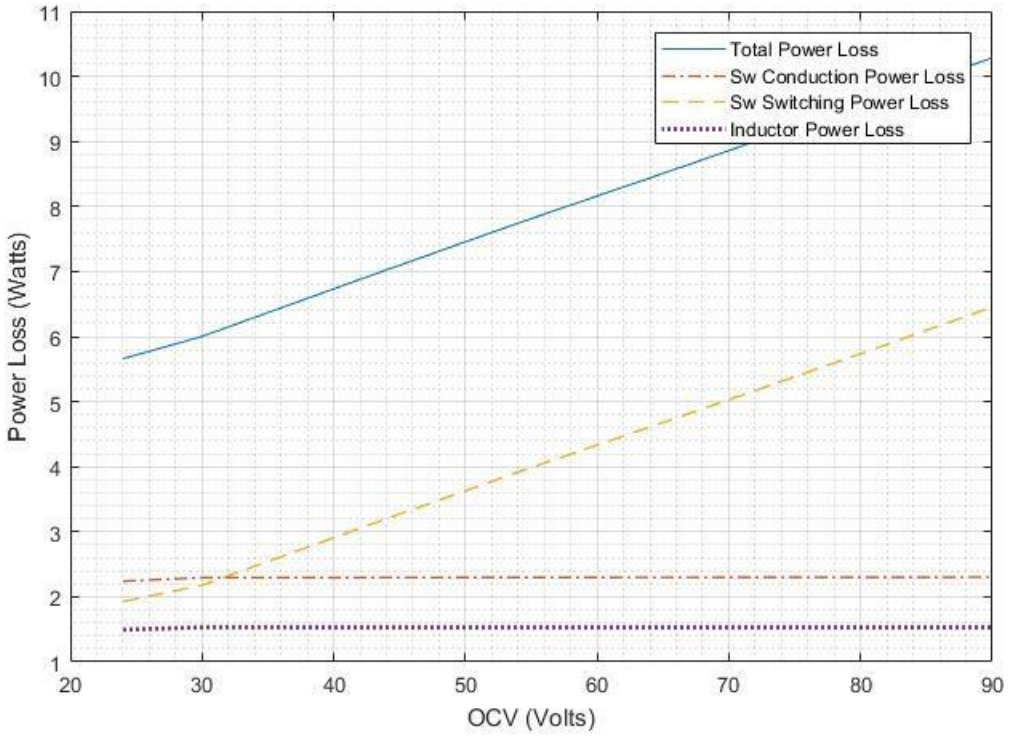

*Figure 25: Buck Converter Losses at 200*W

4.2.3 Boost Converter Losses

Due to the circuit design of the boost converter (Figure (26)) the inductor is placed on the input side of the half bridge. This implies that the inductor current will always be equal to the input current which is usually high in the case of boost converters.

The sum of the switch currents will be equal to the inductor current. This means the conduction losses for the boost converter will be significantly higher compared to the switching losses. This can be shown in Figure (27)

Figure (27) also shows that as the input voltage increases the current decreases the conduction losses decreases until it reaches Open Circuit Voltage (OCV) 24*V* or an input voltage of 12*V,* which is equal to the output voltage. The boost converter cannot go beyond this

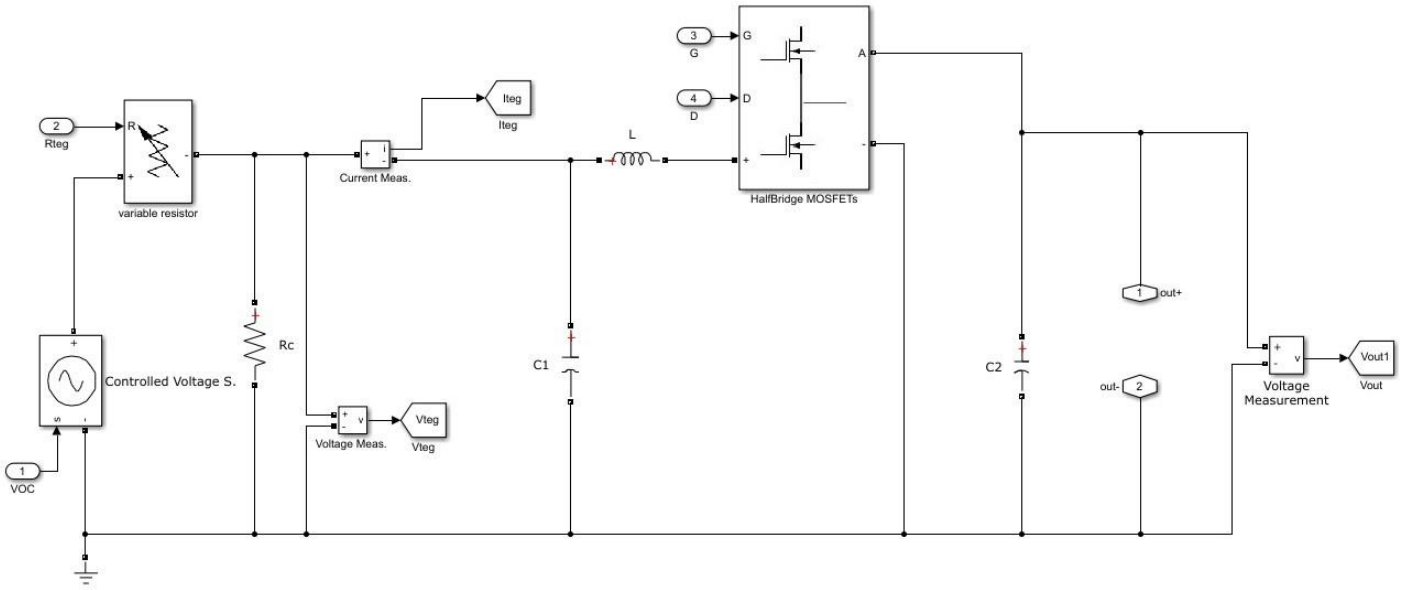

Figure 26: Boost Converter with MOSFET Power Loss Model

point as the duty ratio is approximately equal to zero, where the output and input voltages are equal.

The Figure also shows this relation for different values of power. The lower power values will have lower losses as the current values which effect the conduction losses are lower.

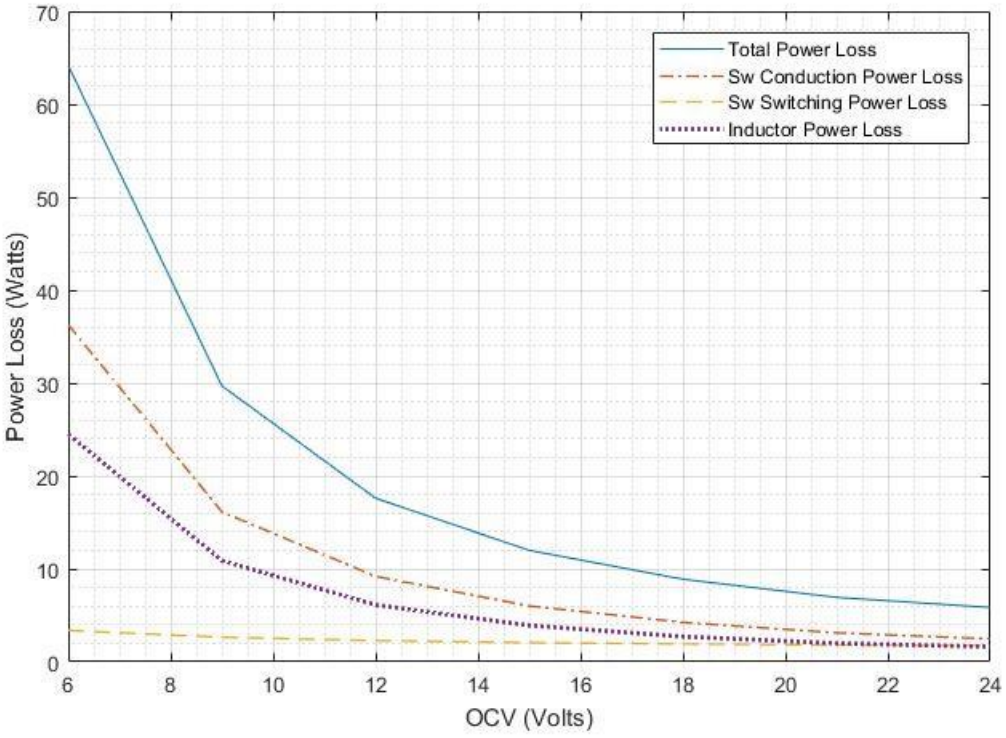

Figure 27: Boost Converter Losses at 200W

4.2.4 SEPIC Converter Losses

The SEPIC converter is a special configuration of the buck-boost converter, it can step up or down the voltage, however it does not invert the output voltage such as the other buck boost configurations. While the original buck-boost converter topology will have similar losses trend as the SEPIC without accounting the resistance of the inductors. The SEPIC was chosen for the analysis of the buck-boost configurations because it is more practical and commonly used due to its ability to preserve the output voltage polarity.

The SEPIC converter includes two inductors in its circuit (Figure (28)). One is on the input side and the other is on the output side. Depending on the duty cycle ratio the utilization of each inductor will vary and thus the losses. This will make the buck-boost topologies less efficient in the case of bucking compared to a buck converter and boosting compared to a boost converter.

However, the minimum losses point will not necessarily be at the output voltage point, this can be shown in Figure (29).

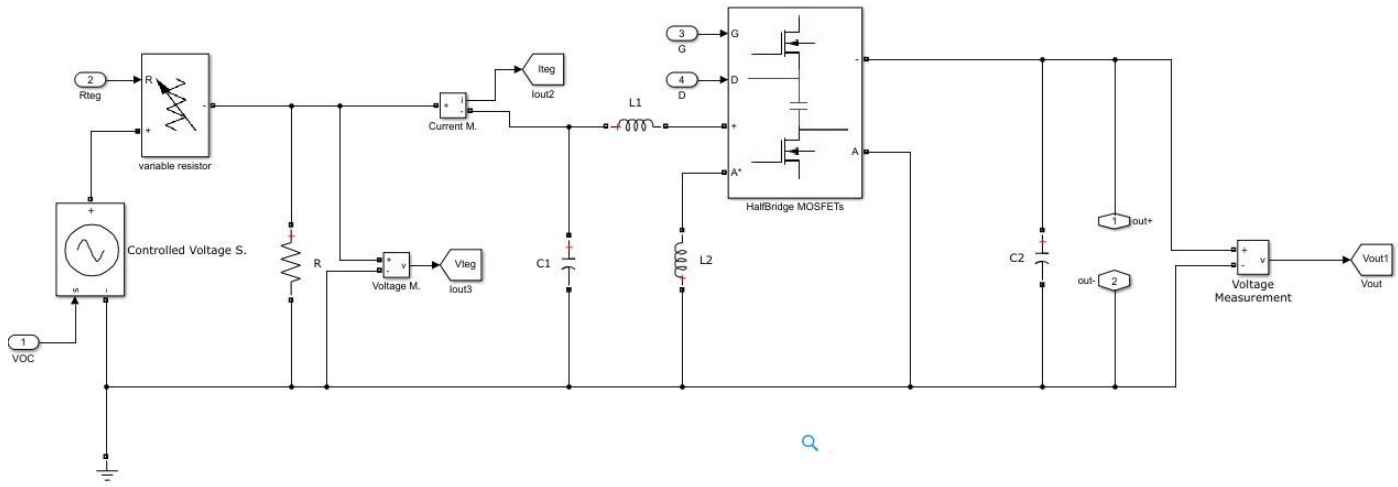

Figure 28: SEPIC Converter with MOSFET Power Loss Model

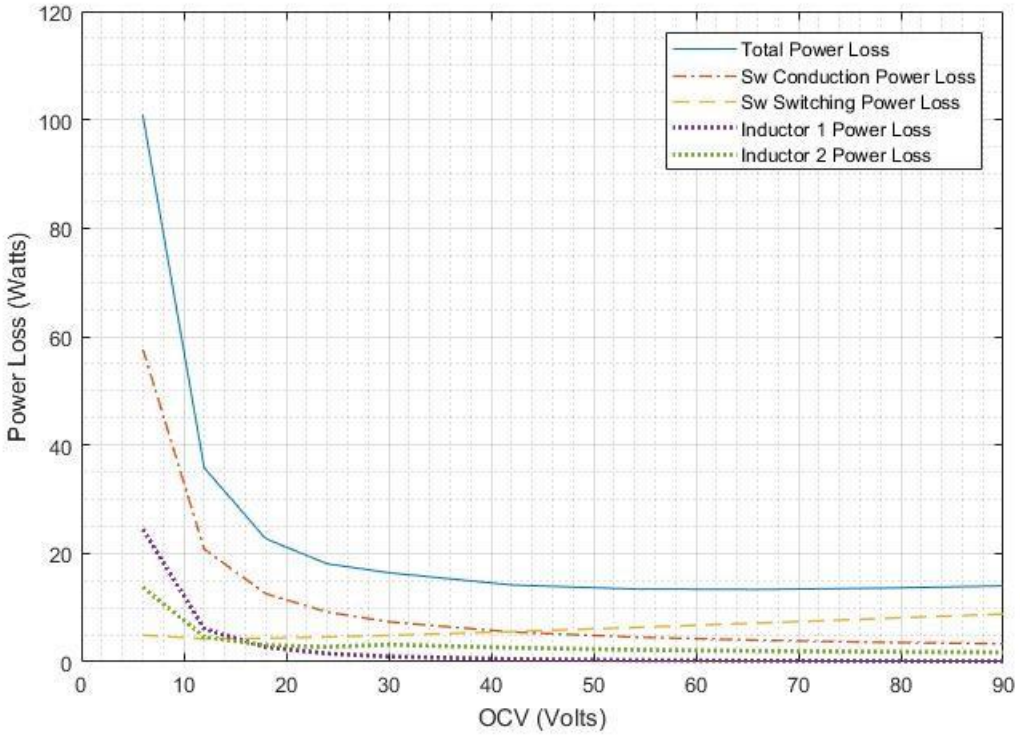

Figure 29: SEPIC Converter Losses at 200W

4.2.5 TEG Configuration Based on Losses

Figure (30) shows combined curves for the buck converter and the boost converter simulation results. The boost being the values lower than 24*V* OCV and the buck being the values higher than 24V.

For this operation where the output is at 12*V* and this type of MOSFET it appears at first glance that operating in the buck region is preferable. Based on this graph a TEG configuration with a combined OCV value of 24*V* without the converters switching at all would be the best case. If

not possible then choosing a configuration on the buck side and close as possible to 24*V.*

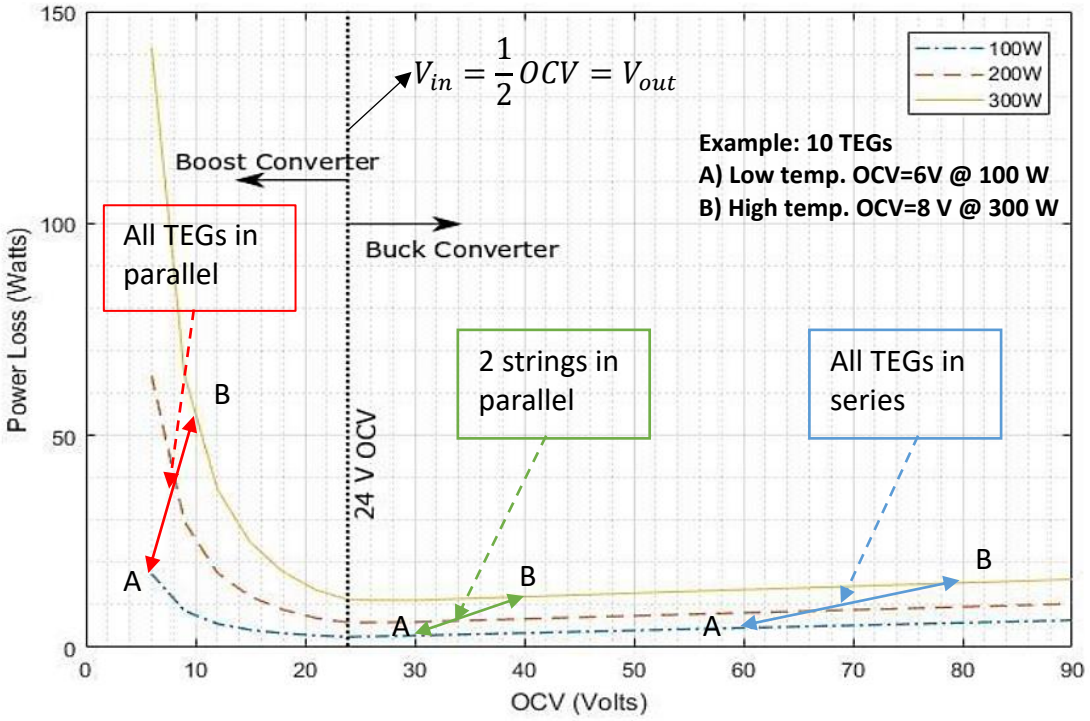

Figure 30: Buck and Boost Converters Losses at Different Power Levels.

However, in a real case scenario the system would not operate at a specific point due to the changing operating conditions as such the power output of the TEG system will change accordingly. As an example, assuming a TEG system consisting of ten TEGs and operate between two power levels due to the change of the temperature difference between the exhaust gas and coolant inside the heat exchanger. The first point (A) is at low temperature difference where each TEG outputs an Open Circuit Voltage ($OCV = 6\,V$) and the combined power of the TEG system is ($P = 100\,W$). The second point (B) is at high temperature difference where each TEG outputs an Open Circuit Voltage of ($OCV = 8\,V$) and the combined power of the TEG system is ($P = 300W$). Depending on which configuration is used to connect the TEG modules, the operating area of the system is determined as shown in Figure (30).

When all the TEG modules are assumed to connect in parallel, a boost converter will be required to step up the voltage to $12\ V$ and the operating area between point (A) and (B) will be as shown by the red colored range. If the TEGs are connected all in series instead, a buck converter will be required to step down the voltage to $12\ V$ and the operating area is shown by the blue colored range. If the TEGs are connected in a combination of two strings in parallel where each string consists of five TEGs in series the operating area is shown by the green colored range.

From this simple example it can be shown what are the power losses of each case and a decision can be made for which configuration to be used. For this example, operating in the buck range is preferable so the series and the two string configurations are feasible. However, other factors must be considered as well. The difference in power may not be considerable between these two configurations however when such a TEG based system operates on a continuous daily basis this small difference in power loss may be considerable on the long term.

Another point to take into consideration is how close the operating range is to the limit of the converter. For the two-string configuration case the operating range is close to the $24\ V\ OCV$ point. If for any reason the system went below this point the buck converter will stop operating and no power would be generated to the DC- microgrid so it might be safer to choose the series connection in this case.

Figure (31) shows the curves for the SEPIC converter simulation results. Due to the way buck boost converters operate in general, where the switch currents are the sum of the input and output currents. The total loss is usually greater than a single buck or a single boost converter.

The minimum value for the losses is also not fixed at $24V$ OCV and changes with different levels of power. However, as shown in Figure (29) the values of the losses seem to slowly change while the SEPIC is in the bucking mode compared to the boosting mode.

Using a SEPIC or the Buck-Boost converter is not necessarily an efficient solution because it will in most cases have more losses. However, some applications may need this topology, such as applications operating at different power levels. which may force the SEPIC converter to operate in boost mode. However, for such applications trying to design the TEG configuration to operate

at buck mode or at *OCV* > 24*V* at normal operation is preferable. It can be concluded that the choice of a TEG configuration or a DC converter is a case by case problem.

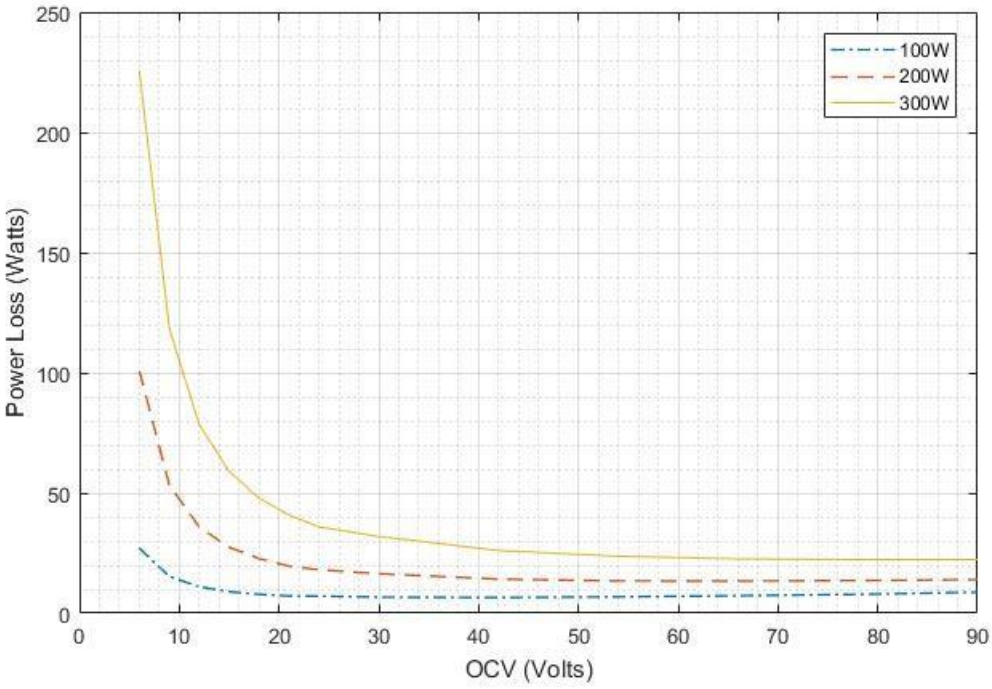

Figure 31: SEPIC Converter Losses at Different Power Levels.

4.3 DC Micro-Grid Case Studies

4.3.1 Introduction

Two case studies are simulated in this section. The objective is to study the effect of battery protection and load shedding modes along with the changing of the battery capacity on the energy harvested and utilized by the micro-grid. The first case study is for a *state of charge limit* = 50% and the second is for a *state of charge limit* = 30%. Additionally, as discussed in section 2.5.1, the tradeoff of using a larger state of charge limit (Depth of Discharge) for the battery lifetime is shown as a cost per energy relation.

4.3.2. Case Study Initial Conditions, Inputs and Load Profiles

For this case study the loads and the inputs for the system were estimated to a profile as a representation of a similar system in the P.O.W.E.R. project. The operation of this case study is assumed to repeat on a daily basis. The inputs are provided in a per hour steady state values and the simulation is assumed to be a steady state.

The load profile in Figure (32) always has a necessary load of 50W that is needed to keep the waste heat recovery system running, the rest of the load profile follows a general representation of a restaurant where the electric power usage increases during day operation and is maximum at night time.

For the TEG/HX system, the temperature profile shown in Figure (33) for the exhaust gas was set like an oven operation in a restaurant where the oven is left operating at a low temperature while the restaurant is closed, and the high temperature range is during the oven operation.

Some values are assumed constant for the TEG/HX model are the gas mass flow rate $\dot{m}_{gas} = 0.06\ kg/sec$, the water flow rate $\dot{Q}_{water} = 10\ L/min$, the cold-water inlet temperature assumed to be constant at $T_{water} = 60\ °C$.

The initial condition for the battery state of charge is $SOC = 50\%$ for the first case and $SOC = 30\%$ respectively. These are also their lower limits as the system will prevent going below these values.

The test is repeated for several battery capacities ranging from $c = 30\ A.h.$ to $c = 110\ A.h.$ with steps of $10\ A.h.$ for each iteration.

For the choice of a DC converter topology to be used in the MPPT, it is known that the loads are operating at an output voltage at 12V. The TEG/HX system was set to always generate voltage to the system higher than 12V so the converter required will always operate in step down mode. A buck converter was chosen for this case study.

The case studies are design such that the total energy generated from the TEG system is equal to the total energy needed by the load so that the total energy utilized in the study can be set to

a value. It was also designed at low battery capacities to show some of the battery protection modes mentioned in Section 3.7.

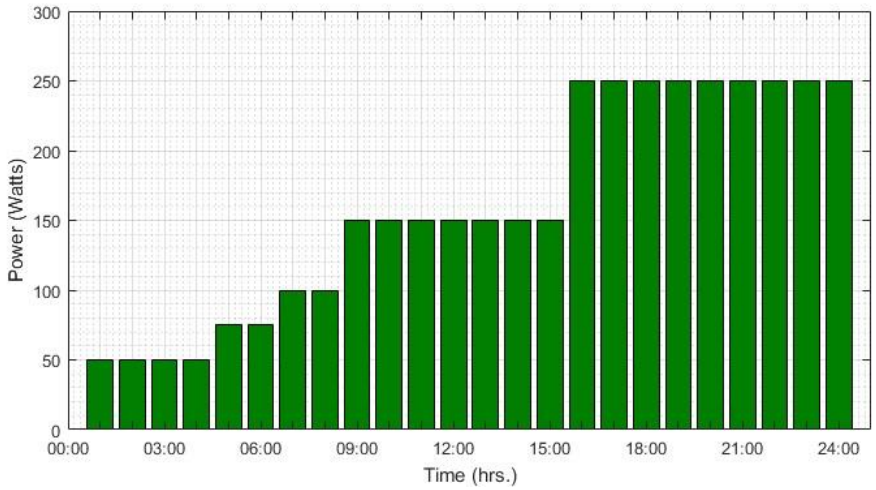

Figure 32: Load Profile for the electrical side of the system

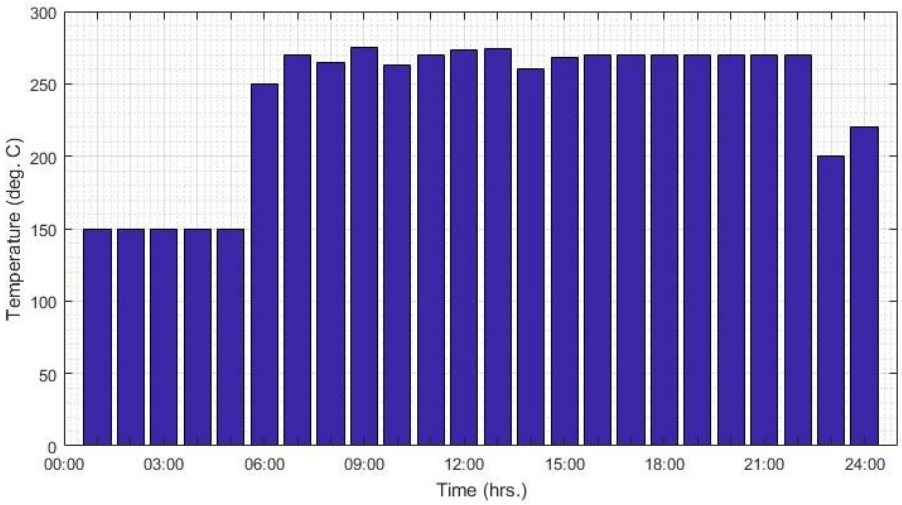

Figure 33: Temperature Profile for the exhaust gas inlet to the heat exchanger

4.3.3 Model Predictions and Energy Savings

Figures (34) and (35) shows the per hour power generated from the TEG/HX P_{TEG}, the Output of the MPPT including the losses P_{Out} , the power demand of the loads P_{Load}, the power discharge from or charged to the battery P_{Bat} , and the *SOC* of the battery during operation. Normally, P_{TEG} is generating enough power so that P_{Out} is greater than the load and P_{Bat} is charging the battery or P_{TEG} is not generating enough power and P_{Out} is less than P_{Load} so the battery discharges with P_{Bat} to balance the total power.

However, the four-different battery protection and load shedding scenarios studied in section 3.7 may occur and before discussing them for this case study it is important to mention that the power values in these Figures are only for the beginning of each hour of the 24 hours. Any power changes during these hours because of the mentioned scenarios may not be shown in the Figures. However, they are calculated and taken into consideration when simulating the battery SOC and the total energy utilized which is discussed in the next section.

The first is Over Charge Protection mode, when P_{Out} is greater than P_{Load} so the battery is charging but it reaches the maximum threshold as shown in Figure 4.11a between hours 10: 00 − 15: 00 and Figure 4.12a between hours 13: 00 − 15: 00. In this scenario the MPPT will diverge from the maximum power point of the TEGs so that P_{Bat}= 0 and avoid overcharging, the graph shows in some cases P_{Bat} not equal to zero because in previous hours the MPPT is not exactly equal to zero, so the battery slightly discharges below the threshold and the model at the beginning of that hour operates normally.

The second scenario is the Under-Charge Protection mode. When P_{Out} is less than P_{Load} so the battery is discharging, but it reaches the lower threshold as shown in Figure (34-a) between hours 23: 00 − 24: 00 and Figure 4.12a at hour 24: 00. In this scenario the system will shed loads so that the power demand will be equal to $P_{Out}$and P_{Bat} = 0. For Figures (34-a) and (35-a) at

hour 23: 00 and 4.12a at hour 24: 00 at the beginning of these hours the battery SOC was above the threshold so the model was operating normally before switching to under charge mode.

The third and fourth scenarios are the Over Charge and Discharge protection. When P_{Out} is greatly higher or lower than P_{Load} so that P_{Bat} exceeds its maximum threshold, the system will start either to divert from the maximum power point or to load shed so P_{Bat} is within the intended limits to protect the battery. The power threshold for Figures (34-a) and (35-a) is $P_{th} = 0.2C * V_{Bat} = 0.2 * 60 * 12 = 144\ W$ so this mode was not activated for these case studies.

Figures (34-b) and (35-b) maintain normal operation and do not switch to any of the mentioned modes as the battery capacity was sufficient to store all the excess power from the system and provide it back to the load when necessary. The per hour power shown in the Figures is equal to the energy generated for one hour. To calculate the energy utilized by the load for the whole day in such case studies the values of each hour for the load energy is summed together.

$$E_{Utilized} = \sum_{h=0}^{h=24} E_{Load}\ \ kW.h \tag{4.3}$$

The total energy utilized relation with the battery capacity is shown later in Figure (38).

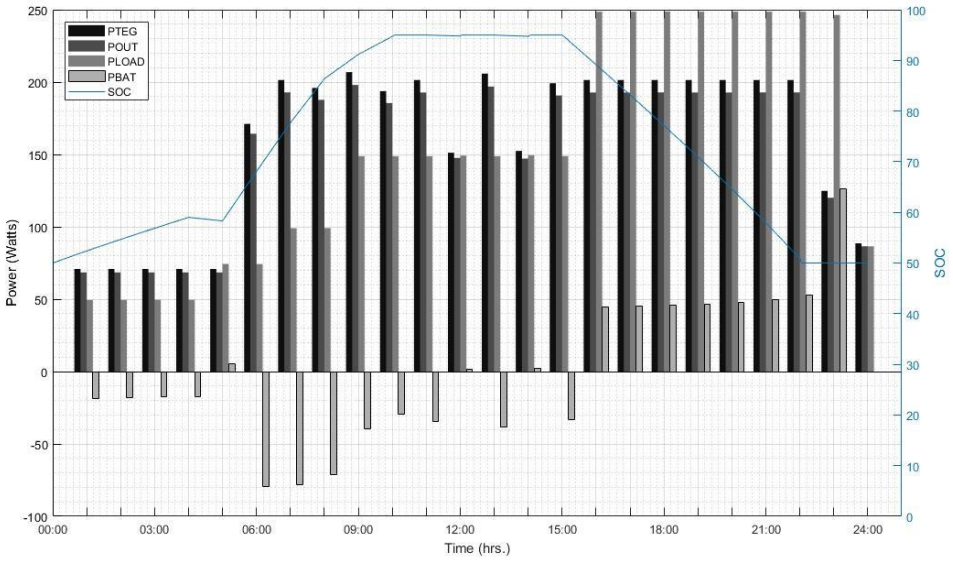

(a) Battery capacity 60*Ah*.

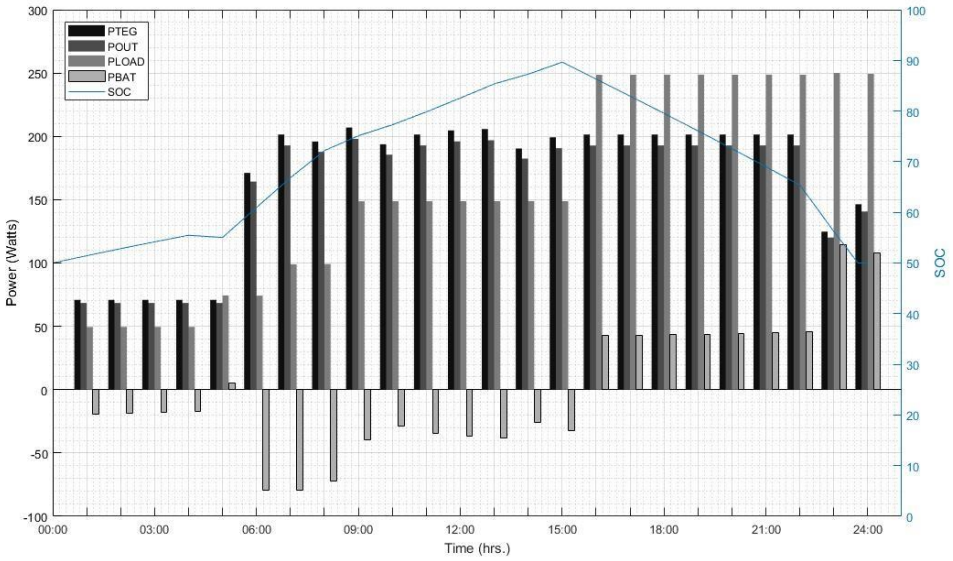

(b) Battery capacity 100*Ah*.

Figure 34:Power generated per hour for the TEGs, MPPT, Loads and Battery with battery state of charge for different battery capacities at state of charge limit 50%, c = 60,100Ah.

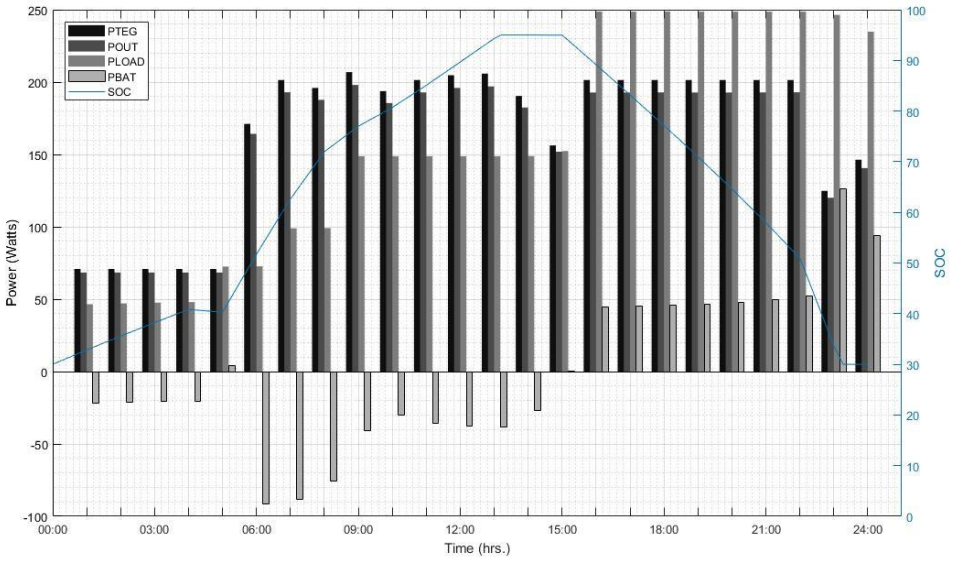

(a) Battery capacity 60*Ah*.

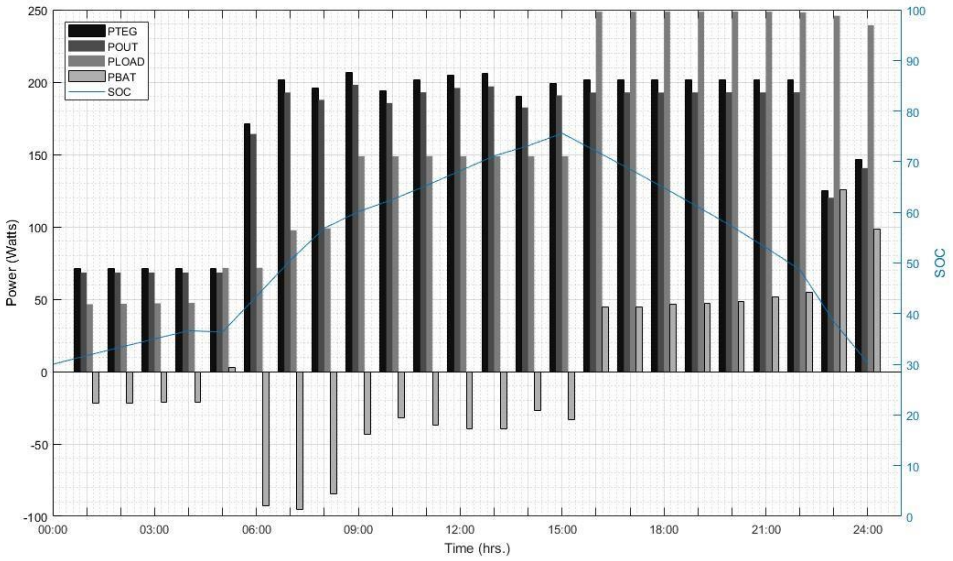

(b) Battery capacity 100*Ah*.

Figure 35: Power generated per hour for the TEGs, MPPT, Loads and Battery with battery state of charge for different battery capacities at state of charge limit 70%, c = 60,100Ah.

This section below shows the per hour performance of the DC microgrid for the two case studies at 50% State of Charge Lower Limit and 30% State of Charge Lower Limit. However, it includes battery capacities starting from 50 A.h., up to 110 A.h. with steps of 10 A.h. between each graph. This allows a close comparison between the different battery capacities.

50% State of Charge Lower Limit (50% Depth of Discharge)

Figures [36] (a-g), shows that with increasing battery capacity the more the dc-microgrid can utilize the energy generated by the TEGs at the excess periods to compensate for the periods of insufficient energy generation. Starting from 90 A.h. the battery system is able to fully utilize the TEGs energy for this case study. Increasing the batter capacity beyond this value will be oversizing it for this system requirements.

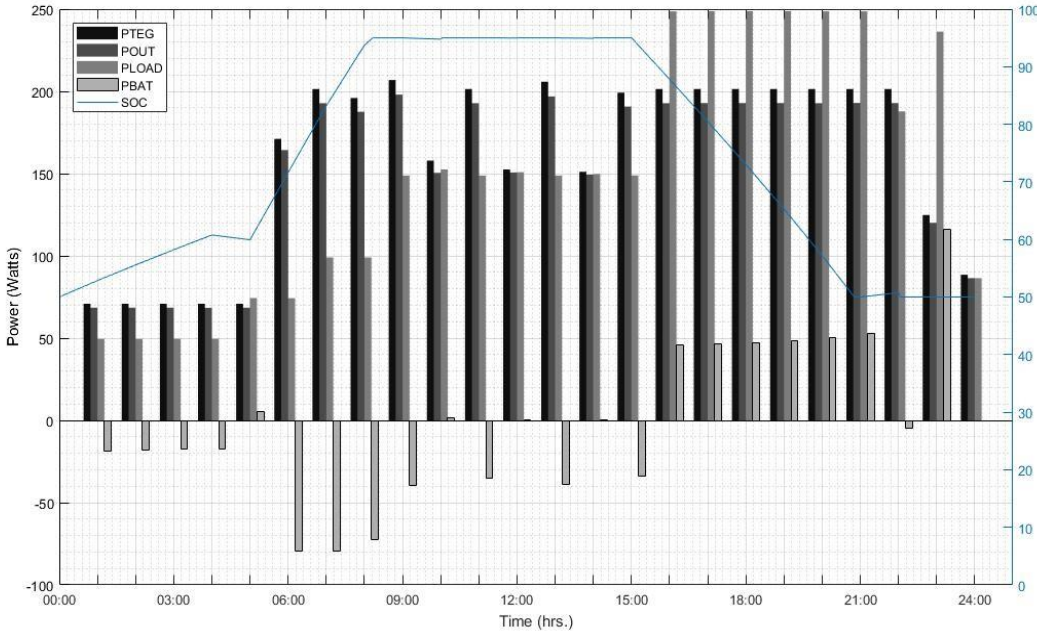

(a) Battery Capacity = 50 A.h.

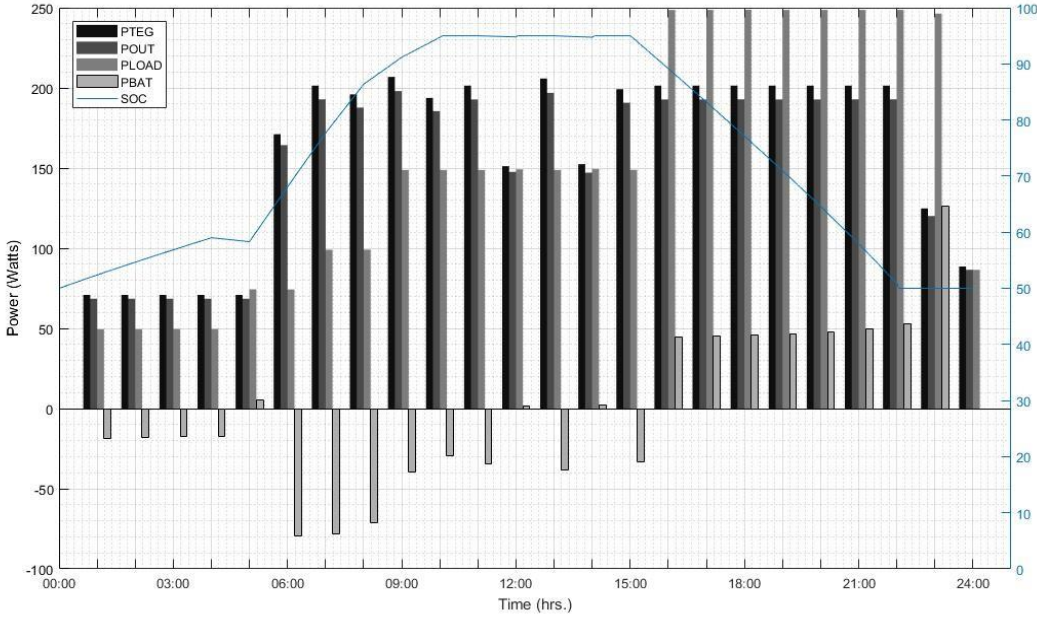

(b) Battery Capacity = 60 A.h.

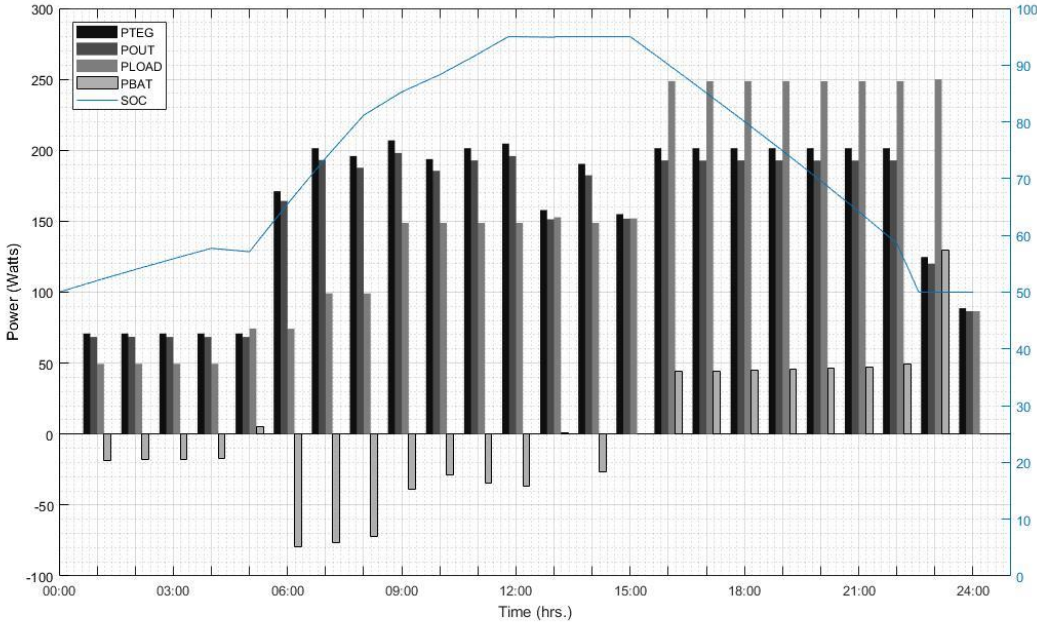

(c) Battery Capacity = 70 A.h.

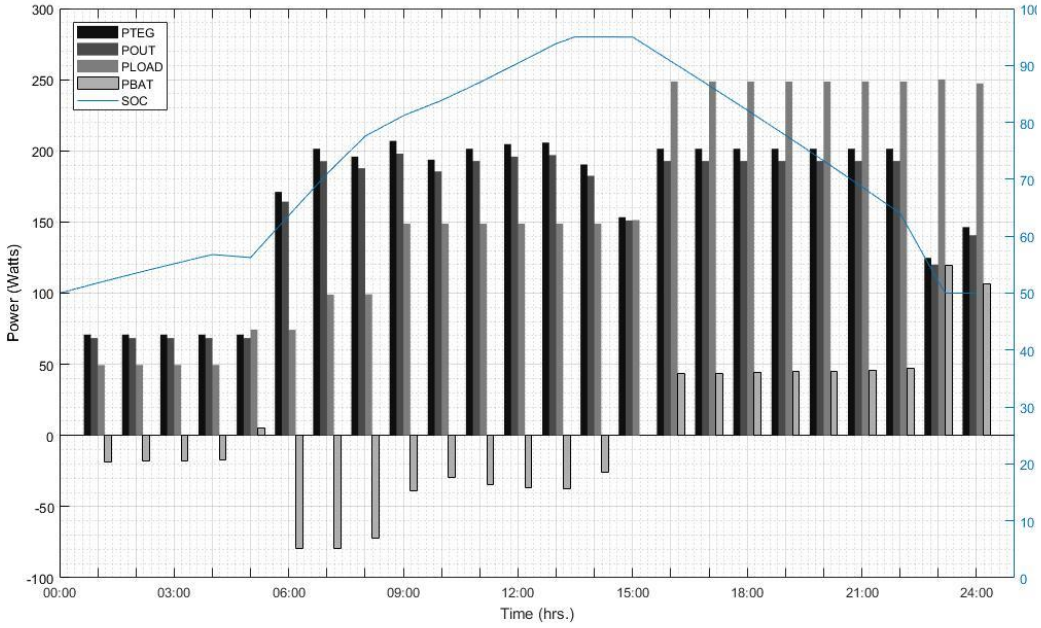

(d) Battery Capacity = 80 A.h.

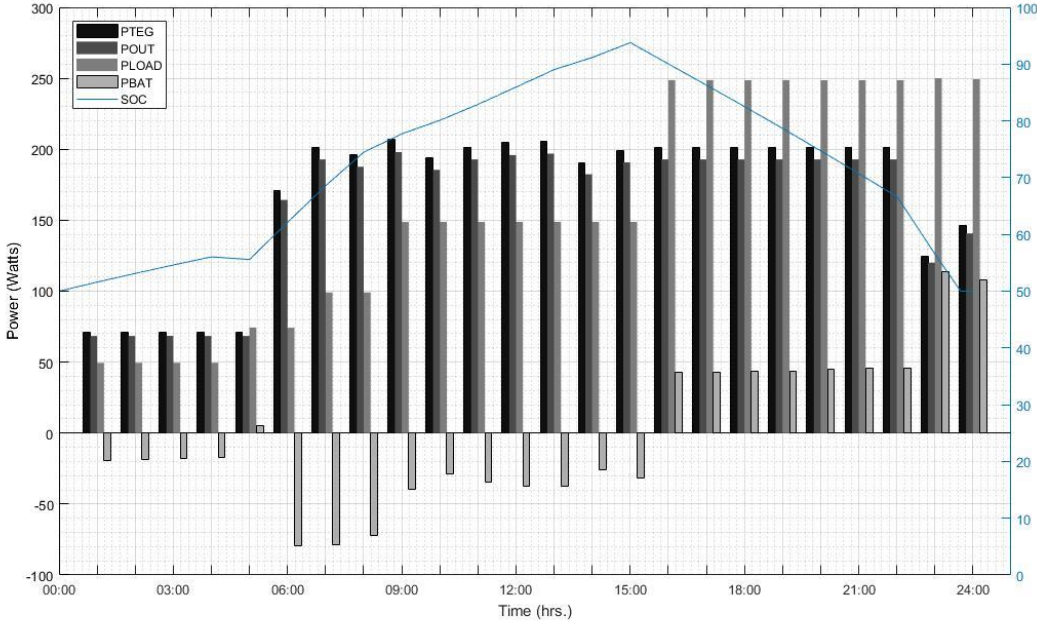

(e) Battery Capacity = 90 A.h.

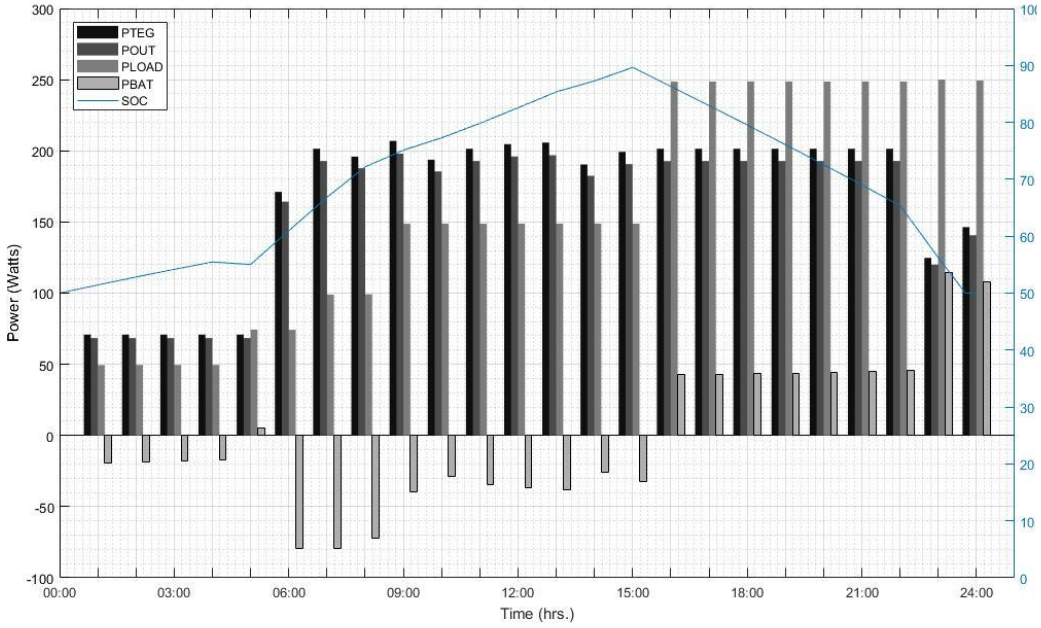

(f) Battery Capacity = 100 A.h.

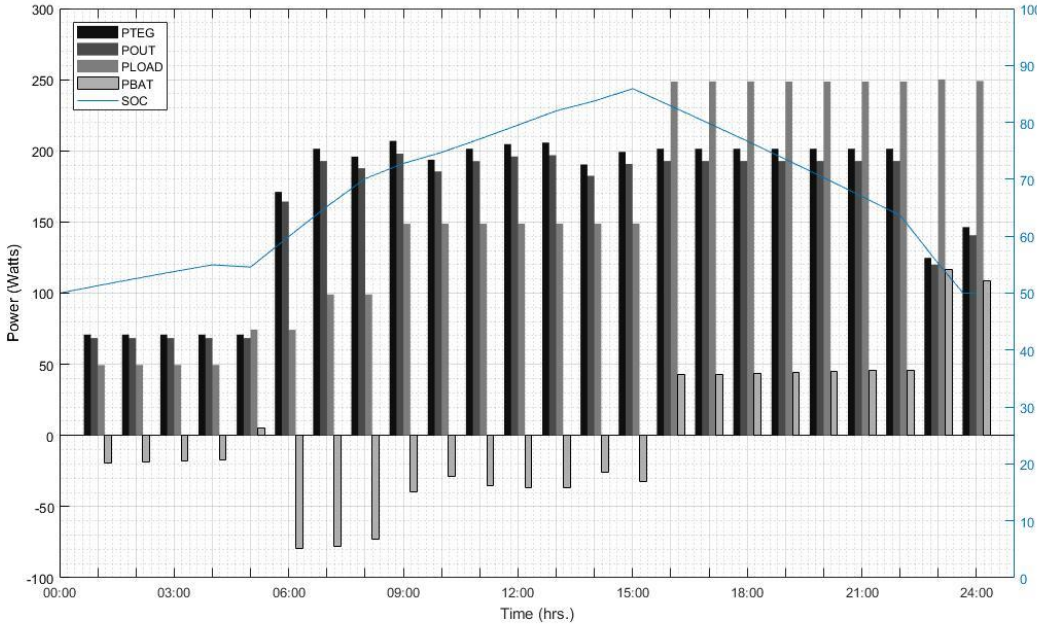

(g) Battery Capacity = 110 A.h.

Figure 36: (a-g) Power generated per hour for the TEGs, MPPT, Loads and Battery with battery state of charge for different battery capacities at state of charge limit 50%.

30 % State of Charge Lower Limit (70% STATE OF CHARGE LIMIT)

Figures [37] (a-g), like the first case shows that with increasing battery capacity the more the dc- microgrid can utilize the energy generated by the TEGs at the excess periods to compensate for the periods of insufficient energy generation. However, due to the higher state of charge limit the battery capacity required to dully utilize the energy generated by the TEGs is lower at 70 A.h., Increasing the capacity beyond this value is oversizing the battery to this system.

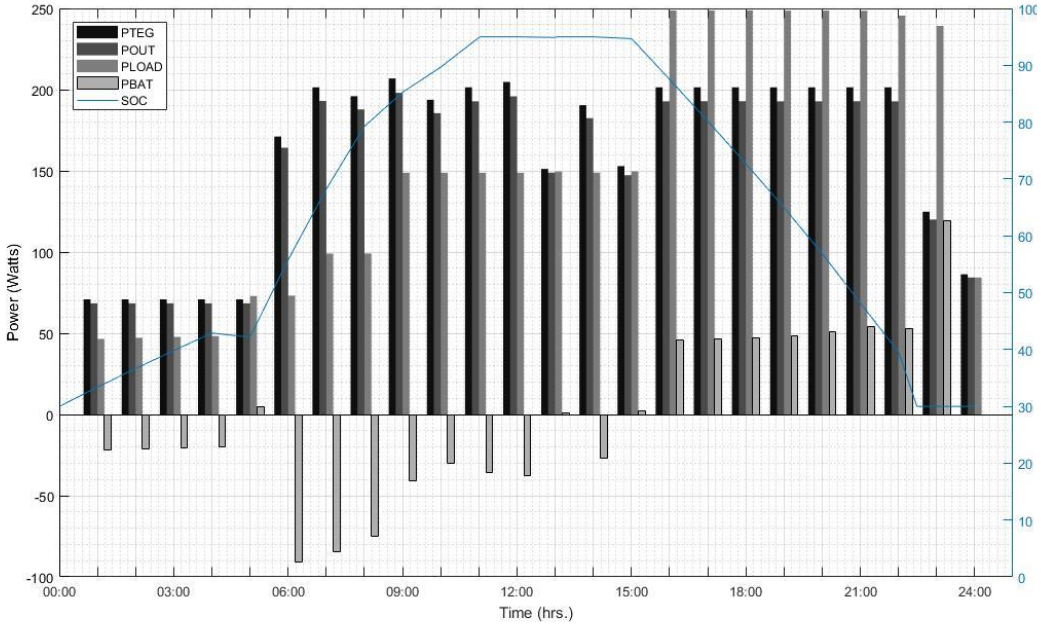

(a) Battery Capacity = 50 A.h.

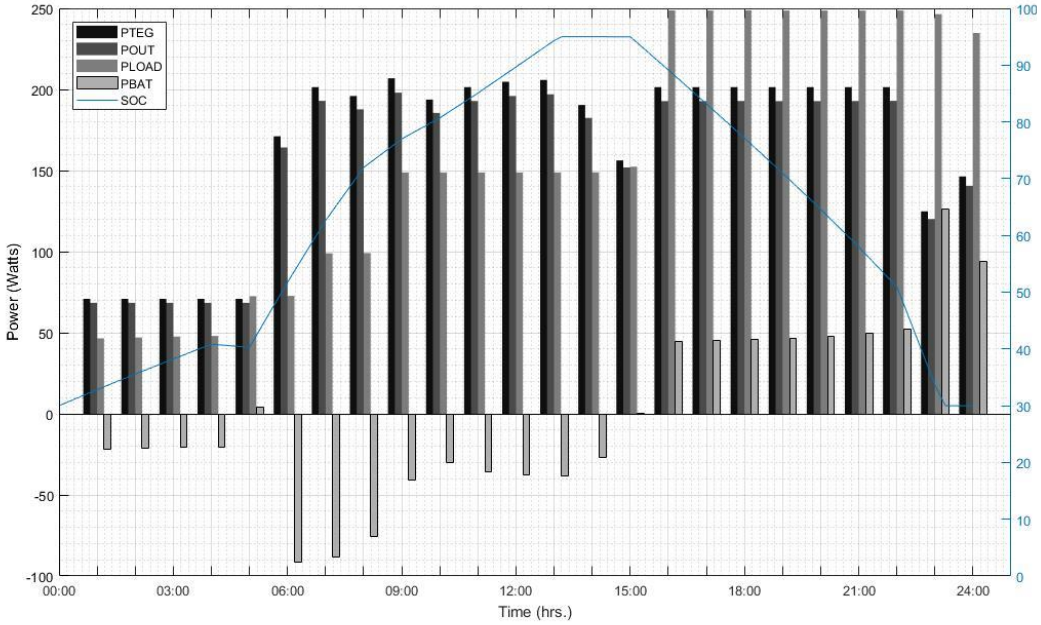

(b) Battery Capacity = 60 A.h.

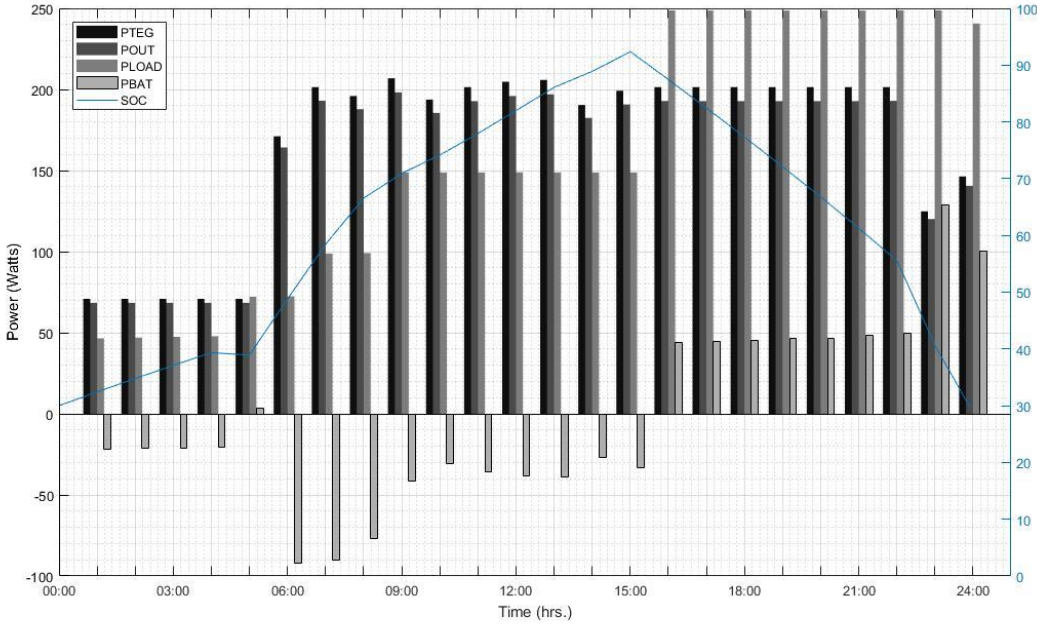

(c) Battery Capacity = 70 A.h.

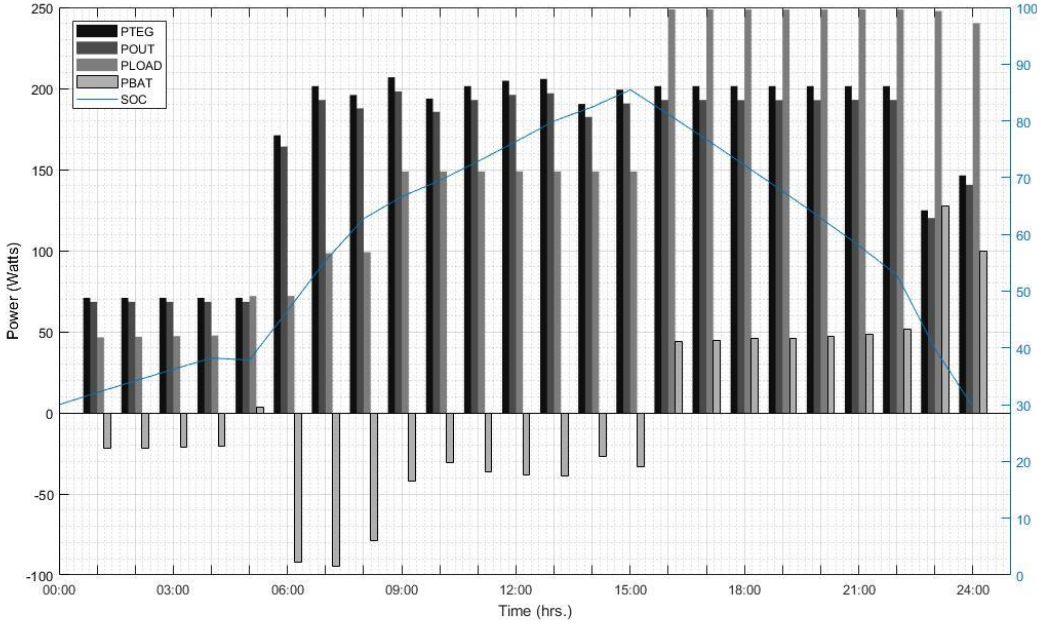

(d) Battery Capacity = 80 A.h.

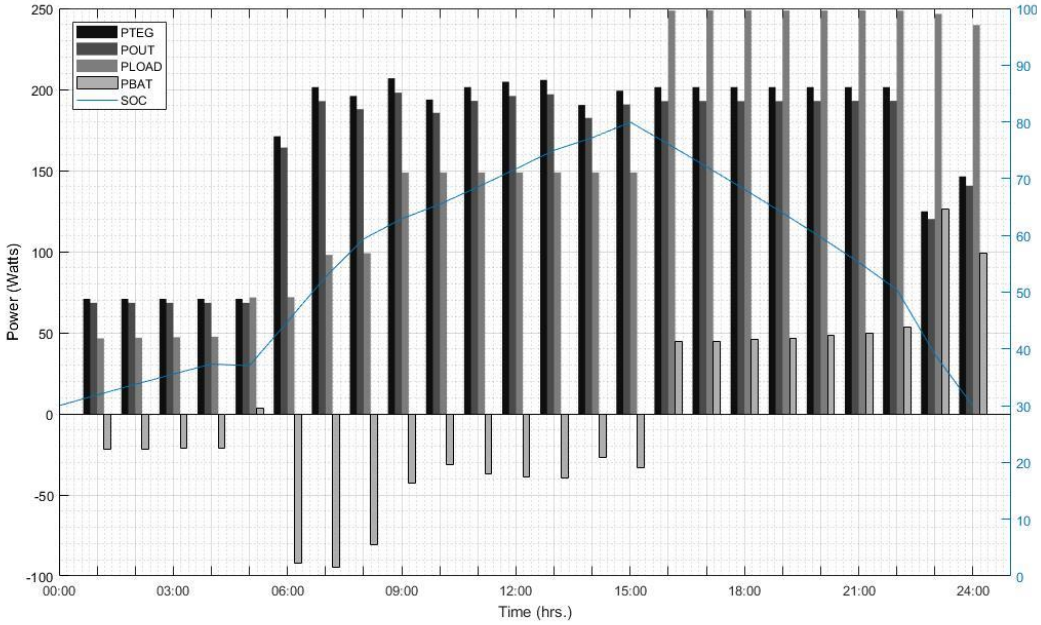

(e) Battery Capacity = 90 A.h.

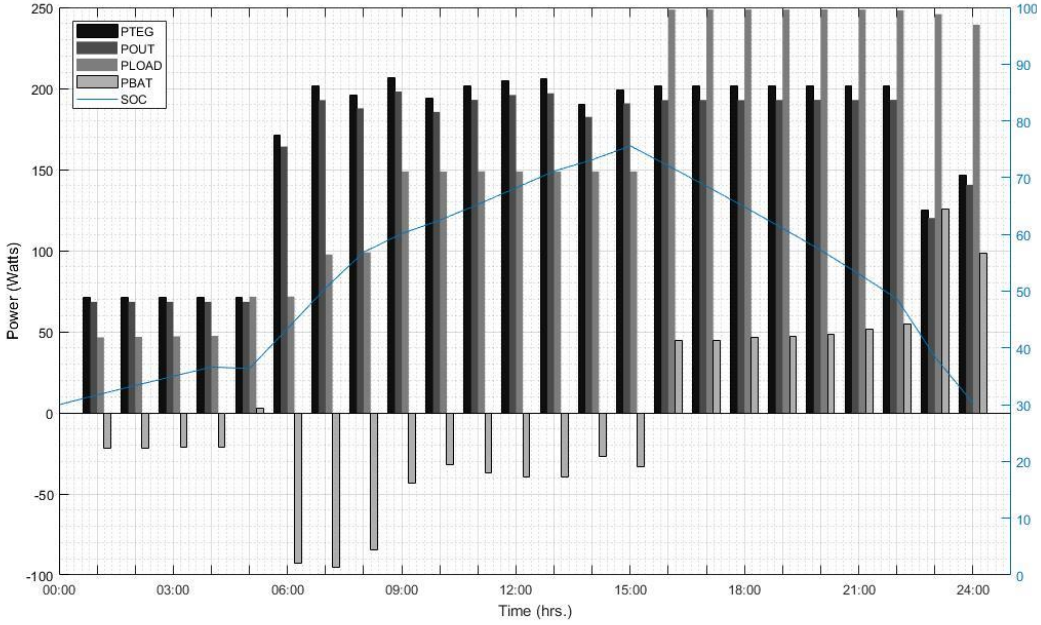

(f) Battery Capacity = 100 A.h.

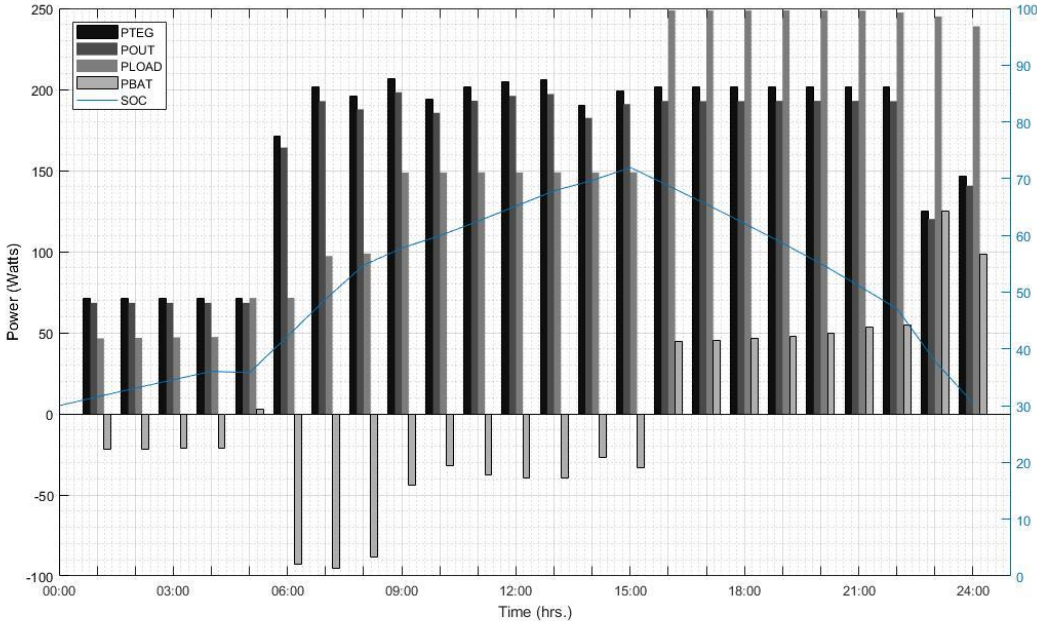

(g) Battery Capacity = 110 A.h.

Figure 37: (a-g) Power generated per hour for the TEGs, MPPT, Loads and Battery with battery state of charge for different battery capacities at state of charge limit 30%.

From all the battery capacity ranges (50 A.h. to 110 A.h.) tested on both case. It was possible to get a relation between the energy utilized, the STATE OF CHARGE LIMIT and the battery capacity. Figure (38) shows the energy utilized per day in relation to the Battery capacity of the system for the two cases of state of charge limit at 50% and 70%. By comparing the two cases using a state of charge limit of 70% will utilize the battery more than the case of 50%, which makes Figure (38-b) saturate at a lower battery capacity.

Using state of charge limit 70% over 50% may seem to be the better solution at first because it will allow the implementation of batteries with lower capacities which translates to lower cost. However, as discussed in section 2.5.1 using a high state of charge limit will affect the battery life time. From Table 2.2 the lifetime of the 70% state of charge limit case will be around 68% of the 50% state of charge limit case.

This means the 70% state of charge limit case will need more frequent maintenance compared to the 50% state of charge limit case. Taking this into consideration, there is a tradeoff between the capacity utilized by the battery, number of batteries used and maintenance cost.

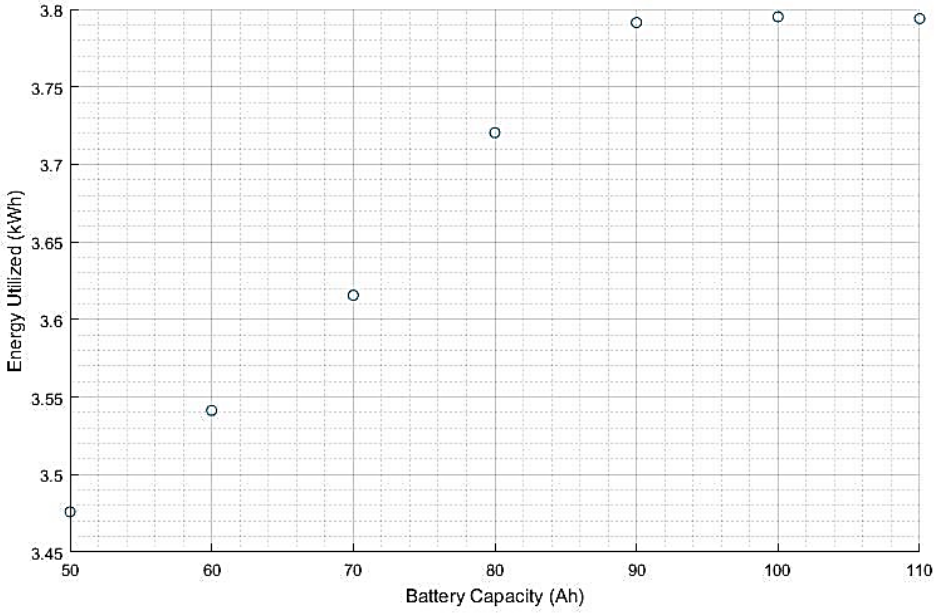

(a) State of charge limit 50%.

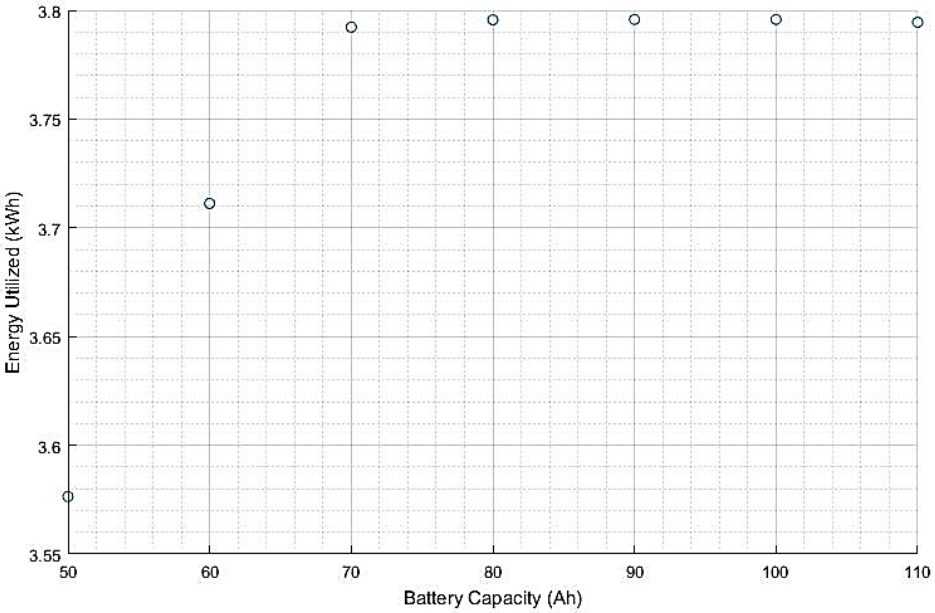

(b) State of charge limit 30%.

Figure 38:Energy Utilized per Day using different Battery Capacities.

4.4. Summary

To minimize the power loss for the DC-micro-grid the power loss for different DC converters were studied, at specific operating conditions where the output voltage is held constant to the load voltage and the input voltage is changing to simulate different TEG configurations. It was shown that each DC converter requires a certain operating configuration. However, for the operating conditions in this study buck converters show more efficient performance due to the low output voltage. Choosing a TEG configuration should be based on the output load voltage. Designing a configuration with operating voltage close to the output voltage reduces the power losses in the MPPT.

A case study was simulated for the system which shows that an isolated DC micro-grid with TEGs as a power source is indeed feasible and conditions which result in system failure or shutdown

can be avoided with load shedding and battery protection modes. The model can also estimate the appropriate battery capacity for such system.

A buck converter was picked for this case study because always during operation the input voltage is higher than the output and the input was steady and did not change over a wide range, it also has lower losses than a SEPIC converter.

Using a higher state of charge limit increases the energy utilized per cycle however a tradeoff study between the battery life cycle, cost and energy savings is needed to determine the optimum battery operating conditions for an application.

Chapter 5

Conclusion and Future Work

5.1. Conclusion

The implementation of an isolated DC-micro-grid for thermo-electric generators (TEGs) as a power source requires certain considerations to maximize the energy harvested from such system. Being the only power source, the electrical system must be able to adapt with the power fluctuations of the TEGs which in turn is dependent on the operation of the heat source for the waste heat recovery system and be able to supply as much of the load demand as possible thus maximizing the utilization of the energy harvested through the system.

There are two main parts for this problem, the first being maximizing the energy harvested during steady state operation, the second is the power management of the system when the power generated and demanded are not equal.

For the steady state operation part, the power losses in the MPPT circuit is studied in relation to the TEG electrical configuration using a power loss model. For a constant output at the load side. The power loss model was implemented for three main types of DC converters Buck, Boost and SEPIC.

Studying the buck and boost converters it was found that to minimize losses it is required to design the TEG system open circuit voltage to a value double of the load side voltage. Thus,

when the MPPT achieves maximum power point the operating voltage across the TEG terminals will be close to the value of the load side. This is shown to be the result of the conduction losses being at its lowest for the boost converter, and the switching losses being at its lowest for the buck converters.

In case of the buck boost or SEPIC converters the total losses decrease as the TEG open circuit voltage increase however it reaches a point where the conduction losses are too small to influence the total losses while the switching losses increases with the TEG operating voltage and the total losses starts to rise again. This is the point of minimum power losses.

For the power management part, the system was designed such that it stores the excess power generated or to compensate for the excess load demand using a battery system. The system can automatically react to conditions where the battery system reaches its limit state of charge which is a value predetermined by the designer to insure a certain life time range for the battery.

A case study was implemented to test the model under different battery capacities and depth of discharge. This shows what is the appropriate battery capacity to use for different system operating conditions to maximize the energy harvested.

The model can be used in selecting a TEG configuration based on the power loss model for the DC converter. It is also able to take into consideration all the system losses starting from the heat exchanger to the loads and simulate the system losses at each stage. This is beneficial in providing estimates for real systems in similar applications to determine their feasibility.

5.2. Future Work

The developed DC-micro-grid model operates on an overall value for the open circuit voltage and short circuit current for the TEG system given from the integrated TEG/HX model, to study other TEG/MPPT configurations such as Distributed MPPT (DMPPT) where an MPPT is connected to each TEG module, string or both, the DC-micro-grid model and the TEG/HX model will need to be adjusted for such systems.

The current study shows the relation of the TEG configurations with the power losses in the DC converters for the MPPT. A further step is to study effects such as temperature mismatch in the TEG system on the overall system performance. Combining this with studying DMPPT systems, one can optimize a system to minimize the overall losses in the thermal TEG and electrical DC micro-grid systems by choosing the appropriate TEG and MPPT configurations.

The developed model could be used for the prediction of a system performance however it's accuracy to a real-life DC microgrid system is not determined. The next step for this model would be the experimental validation and comparison with such a real system. This would allow the model to be used as a benchmark in testing similar real-life waste heat recovery systems before implementation.

References

[1] J. L. Pellegrino, N. Margolis, M. Justiniano, M. Miller, and A. Thedki, "Energy Use, Loss and Opportunities Analysis: US Manufacturing and Mining.," *DOE/ITP (U.S. Dep. Energys Ind. Technol. Program)*, p. 169, 2004.

[2] CESAR, "Sankey diagram of canadas energy systems." [Online]. Available: http://www.cesarnet.ca/%0Avisualization/sankey-diagrams-canadas-energy-systems?scope=Quebec&year=%0A2010&modifier=none&hide=exp&scalevalue=0.17647594672753303#chart-form,.

[3] D. Wang, X. Ling, H. Peng, L. Liu, and L. Tao, "Efficiency and optimal performance evaluation of organic Rankine cycle for low grade waste heat power generation," *Energy*, vol. 50, pp. 343–352, Feb. 2013.

[4] D. Rowe, Ed., *Thermoelectrics Handbook*. CRC Press, 2005.

[5] J. Girard, "The investigation of exhaust control strategies and waste heat recovery practices of naturally-ventilated exhaust streams," p. 179, 2016.

[6] M.Zaher, "The Integration of Annular Thermoelectric Generators in a Heat Exchanger for Waste Heat Recovery Applications."

[7] D. Finnerty, "The Development of Methodologies and a Novel Test Facility for the Characterisation," p. 127, 2013.

[8] Z. B. Tang, Y. D. Deng, C. Q. Su, W. W. Shuai, and C. J. Xie, "Case Studies in Thermal Engineering A research on thermoelectric generator â€™ s electrical performance under temperature mismatch conditions for automotive waste heat recovery system," vol. 5, pp. 143–150, 2015.

[9] A. Montecucco, J. Siviter, and A. R. Knox, "The effect of temperature mismatch on thermoelectric generators electrically connected in series and parallel," *Appl. Energy*, vol. 123, pp. 47–54, 2014.

[10] A. A. Negash, T. Y. Kim, and G. Cho, "Effect of electrical array configuration of thermoelectric modules on waste heat recovery of thermoelectric generator," *Sensors Actuators, A Phys.*, vol. 260, pp. 212–219, 2017.

[11] R. Thankakan and E. R. Samuel Nadar, "Investigation of thermoelectric generators connected in different configurations for micro-grid applications," *Int. J. Energy Res.*, no. January, pp. 1–12, 2018.

[12] G. Spagnuolo, E. Franco, J. D. Bastidas-Rodriguez, C. A. Ramos-Paja, and G. Petrone, "Maximum power point tracking architectures for photovoltaic systems in mismatching conditions: a review," *IET Power Electron.*, vol. 7, no. 6, pp. 1396–

1413, 2014.

[13] X. Zhang, K. T. Chau, C. C. Chan, and S. Gao, "An automotive thermoelectric-photovoltaic hybrid energy system," in *2010 IEEE Vehicle Power and Propulsion Conference*, 2010, pp. 1–5.

[14] "Australian Energy Research Laboratories." [Online]. Available: https://www.aerl.com.au/mppt-solar-charge-controller-history/. [Accessed: 13-Mar-2018].

[15] T. Esram and P. L. Chapman, "Comparison of Photovoltaic Array Maximum Power Point Tracking Techniques," *IEEE Trans. Energy Convers.*, vol. 22, no. 2, pp. 439–449, 2007.

[16] J. J. Schoeman and J. D. Wyk, "A simplified maximal power controller for terrestrial photovoltaic panel arrays," in *1982 IEEE Power Electronics Specialists conference*, 1982, pp. 361–367.

[17] R. M. Hilloowala and A. M. Sharaf, "A rule-based fuzzy logic controller for a PWM inverter in photo-voltaic energy conversion scheme," in *Conference Record of the 1992 IEEE Industry Applications Society Annual Meeting*, pp. 762–769.

[18] T. Hiyama, S. Kouzuma, and T. Imakubo, "Identification of optimal operating point of PV modules using neural network for real time maximum power tracking control," *IEEE Trans. Energy Convers.*, vol. 10, no. 2, pp. 360–367, Jun. 1995.

[19] S. M. A. M. F. N. Tajuddin, M. S. Arif, "Perturbative methods for maximum power point tracking (MPPT) of photovoltaic (PV) systems: a review," *Int. J. energy Res.*, vol. 39, no. February 2015, pp. 1153–1178, 2015.

[20] W. Xiao and W. G. Dunford, "A modified adaptive hill climbing MPPT method for photovoltaic power systems," *PESC Rec. - IEEE Annu. Power Electron. Spec. Conf.*, vol. 3, pp. 1957–1963, 2004.

[21] N. Femia, G. Petrone, G. Spagnuolo, and M. Vitelli, "Optimization of perturb and observe maximum power point tracking method," *IEEE Trans. Power Electron.*, vol. 20, no. 4, pp. 963–973, 2005.

[22] N. Mohan, T. M. Undeland, and W. P. Robbins, *Power Electronics: Converters Applications and Design*, 3rd ed. John Wiley & Sons, Inc., 2003.

[23] S. Munk-Nielsen, L. N. Tutelea, and U. Jaeger, "Simulation with ideal switch models combined with measured loss data provides a good estimate of power loss," *Conf. Rec. - IAS Annu. Meet. (IEEE Ind. Appl. Soc.*, vol. 5, pp. 2915–2922, 2000.

[24] U. Drofenik and J. Kolar, "A general scheme for calculating switching-and conduction-losses of power semiconductors in numerical circuit simulations of power electronic systems," *Int. power Electron. Conf. IPEC-Niigata 2005*, pp. 1–

7, 2005.

[25] S. Fagerstrom and N. Bengiamin, “Modelling and Characterization of Power Electronics Converters Using MATLAB Tools,” *Textbook*, vol. 1, 2012.

[26] M. Mudholkar *et al.*, “Datasheet Driven Silicon Carbide Power MOSFET Model,” vol. 29, no. 5, pp. 2220–2228, 2014.

[27] D. W. Gao, “Sizing of Energy Storage Systems for Microgrids,” *Energy Storage Sustain. Microgrid*, pp. 125–142, 2015.

[28] L. Gaines, “The future of automotive lithium-ion battery recycling: Charting a sustainable course,” *Sustain. Mater. Technol.*, vol. 1, pp. 2–7, 2014.

[29] I. Standard, “IEEE Recommended Practice for Sizing Lead-Acid Batteries for Stationary Applications,” 2011.

[30] P. Ricciuti, “A Thermodynamic Investigation of Commercial Kitchen Operations and the Implementation of a Waste Heat Recovery System,” 2017.

[31] G. Ning and B. N. Popov, “Cycle Life Modeling of Lithium-Ion Batteries,” *J. Electrochem. Soc.*, vol. 151, no. 10, p. A1584, 2004.

[32] G. Sarre, P. Blanchard, and M. Broussely, “Aging of lithium-ion batteries,” *J. Power Sources*, vol. 127, no. 1–2, pp. 65–71, Mar. 2004.

[33] D. U. Sauer and H. Wenzl, “Comparison of different approaches for lifetime prediction of electrochemical systems-Using lead-acid batteries as example,” *J. Power Sources*, vol. 176, no. 2, pp. 534–546, 2008.

[34] D. Doerffel and S. A. Sharkh, “A critical review of using the Peukert equation for determining the remaining capacity of lead-acid and lithium-ion batteries,” *J. Power Sources*, vol. 155, no. 2, pp. 395–400, 2006.

[35] Y. Zhang, H. J. Jia, and L. Guo, “Energy management strategy of islanded microgrid based on power flow control,” *2012 IEEE PES Innov. Smart Grid Technol.*, no. 20090032110064, pp. 1–8, 2012.

[36] A. Luna, L. Meng, N. Diaz Aldana, M. Graells, J. Vasquez, and J. Guerrero, “Online Energy Management Systems for Microgrids: Experimental Validation and Assessment Framework,” *IEEE Trans. Power Electron.*, vol. 33, no. 3, pp. 1–1, 2017.

[37] M. Tasdighi, P. Jambor Salamati, a Rahimikian, and H. Ghasemi, “Energy management in a smart residential building,” *Environ. Electr. Eng. EEEIC 2012 11th Int. Conf.*, pp. 128–133, 2012.

[38] D. Graovac, M. Pürschel, and K. Andreas, “MOSFET Power Losses Calculation Using the Data- Sheet Parameters,” *Infineon Technol. AG*, no. July, pp. 1–23, 2006.